Molecular Therapy
Oncolytics
Original Article

Dual targeting of EZH1 and EZH2 for the treatment of malignant rhabdoid tumors

Haruka Shinohara,[1] Rie Sawado,[1] Makoto Nakagawa,[1,2] Ayuna Hattori,[1,3] Kazutsune Yamagata,[1] Kimiharu Tauchi,[1] Jumpei Ito,[1,4] Yasumichi Kuwahara,[5] Tsukasa Okuda,[5] Chitose Ogawa,[6] and Issay Kitabayashi[1]

[1]Division of Hematological Malignancy, National Cancer Center Research Institute, 5-1-1 Tsukiji, Chuo-Ku, Tokyo 104-0045, Japan; [2]Department of Orthopaedic Surgery, Graduate School of Medical Sciences, Kyushu University, 3-1-1 Maidashi, Higashi-ku, Fukuoka 812-8582, Japan; [3]Department of Biosystems Science, Institute for Frontier Life and Medical Sciences, Kyoto University, 53 Shogoin Kawahara-cho, Sakyo-ku, Kyoto 606-8507, Japan; [4]Department of Pediatrics, Keio University School of Medicine, 35 Shinanomachi, Shinjuku-ku, 160-8582 Tokyo, Japan; [5]Department of Biochemistry and Molecular Biology, Graduate School of Medical Science, Kyoto Prefectural University of Medicine, Kawaramachi-Hirokoji, Kamigyo-ku, Kyoto 602-8566, Japan; [6]Department of Pediatric Oncology, National Cancer Center Hospital, 5-1-1 Tsukiji, Chuo-Ku, Tokyo 104-0045, Japan

Malignant rhabdoid tumors (MRTs) are rare and highly aggressive pediatric cancers with no standard of care. MRTs are characterized by loss of SMARCB1, which results in upregulated expression of enhancer of zeste homolog 2 (EZH2), which is responsible for the methylation of lysine 27 of histone H3 (H3K27me3), leading to the repression of gene expression. Although previous reports suggest EZH2 as an effective therapeutic target, the functions of EZH1, the other homolog of EZH, in MRT remain unknown. Here, we show that EZH1, as well as EZH2, contributes to MRT cell growth and H3K27 methylation. Depletion or selective inhibition of EZH2 led to a compensatory increase in EZH1 expression, and depletion of EZH1 enhanced the effect of EZH2 inhibition. EZH1/2 dual inhibitors suppressed MRT cell growth markedly, reflecting the reduction of H3K27me3 accumulation at one of the EZH1/2 targets, the *CDKN2A* locus. Dual inhibition of EZH1/2 *in vivo* suppressed tumor growth completely, with no significant adverse effects. These findings indicate that both EZH1 and EZH2 are potential targets for MRT therapy, and that EZH1/2 dual inhibitors may be promising therapeutic strategies for MRT.

INTRODUCTION

Malignant rhabdoid tumors (MRTs) are rare and highly aggressive malignancies of infants and young children that occur mainly in the kidney (rhabdoid tumor of the kidney), brain (atypical teratoid rhabdoid tumor [AT/RT]), and soft tissue.[1] While multimodal treatment consisting of surgery, chemotherapy, and radiation has brought modest improvements in overall survival, patients with MRT have a very poor prognosis, with a median survival of around 1 year.[2-4] Consequently, new treatment approaches are needed to improve outcomes.

MRTs are characterized by biallelic inactivation of the tumor suppressor gene *SMARCB1* (also known as *SNF5*, *INI1*, or *BAF47*),[1,5] which encodes a core subunit of the switch/sucrose nonfermentable (SWI/SNF) complex. Loss of SMARCB1 upregulates expression of enhancer of zeste homolog 2 (EZH2).[6,7] EZH2 is one of the components of the catalytic subunit of the polycomb repressive complex (PRC2), which catalyzes methylation of lysine 27 in histone H3 trimethylation (H3K27me3), leading to repression of gene expression.[8] Depletion and inhibition of EZH2 suppress tumorigenesis in *SMARCB1*-deficient cells,[6,7,9-11] suggesting that EZH2 inhibition is a promising strategy for anti-tumor therapy.[12] Although EZH2-selective inhibitors are under evaluation in clinical trials, favorable responses are not observed in all patients.[13]

While EZH2 is recognized as an essential epigenetic regulator in various cancers, recent reports revealed that EZH1, the other homolog of EZH, is also involved in abnormal H3K27 methylation.[14,15] EZH1 co-localizes with H3K27me3 to silence multiple genes associated with transcriptional regulation, proliferation, and differentiation.[14,15] Several small compounds have been developed as EZH1/2 dual inhibitors, and have shown favorable effects against several types of cancer that overexpress or harbor mutations in EZH2 (e.g., adult T cell leukemia-lymphoma, acute myeloid leukemia, and multiple myeloma).[15-19] These reports strongly suggest that EZH1/2 dual inhibitors have efficacy against MRTs; however, the functions of EZH1 in MRT remain unknown. In addition, the therapeutic efficacy of EZH1/2 dual inhibition remains unclear. Here, we investigated the role of EZH1 and EZH2 in MRT and examined the efficacy of EZH1/2 dual inhibitors both *in vitro* and *in vivo*.

RESULTS

Function and expression of EZH1 and EZH2 in MRT cells

Previous reports show that EZH2 is required for cell proliferation and tumor formation in *SMARCB1*-deficient cells[6]; however, the role of EZH1 in MRT cells has not been clarified. Therefore, to elucidate

Received 19 January 2022; accepted 14 September 2022;
https://doi.org/10.1016/j.omto.2022.09.006.

Correspondence: Issay Kitabayashi, Division of Hematological Malignancy, National Cancer Center Research Institute, 5-1-1 Tsukiji, Chuo-Ku, Tokyo 104-0045, Japan.
E-mail: ikitabay@ncc.go.jp

the function of EZH1 and EZH2 in MRT cells, we examined the effects of knockdown (KD) of *EZH1* and *EZH2* using short hairpin RNA (shRNA). Double KD of *EZH1* and *EZH2* reduced H3K27me3 levels more and almost completely and significantly suppressed cell proliferation compared with single KD of each gene (Figures 1A and 1B). These data indicate that both EZH1 and EZH2 are essential for epigenetic regulation and growth of MRT cells. Interestingly, the KD of *EZH2* increased the expression level of EZH1 protein in MRT cells (Figure 1B), which occurred independently of the shRNA target sequences (Figure S1C). A strong increase in levels of *EZH1* mRNA was also observed in A204.1 cells, but there was a lesser or no increase in G401.6TG and TTC642 cells (Figures S1C and S1D). These data suggest that depletion of *EZH2* results in a compensatory increase in EZH1 expression. Based on these findings, we speculated that dual inhibition of EZH1 and EZH2 could efficiently reduce H3K27me3 levels and suppress MRT cell growth.

Dual inhibition of EZH1 and EZH2 in MRT cells

To investigate the effects of chemical dual targeting of EZH1 and EZH2 in MRT cells, we treated five MRT cell lines with the EZH1/2 dual inhibitor DS-3201b, the partially selective inhibitors UNC1999 or CPI-360, or the EZH2-selective inhibitors GSK126 or EPZ-6438 (Figure S2A). The half-maximal inhibitory concentration (IC_{50}) values of these EZH inhibitors against EZH1/2 and H3K27me3 were confirmed previously (Figure S2B).[9,15,18-21] Anti-proliferative effects were observed in MRT cells at 7 to 10 days post-exposure to inhibitors in a dose-dependent manner (Figures 2A and S2C). Of note, the EZH1/2 dual inhibitor reduced MRT cell growth more strongly than the EZH2-selective inhibitors or partially selective inhibitors, although there was a difference in sensitivity (Figures 2A and S2C). The IC_{50} values of these EZH inhibitors for each cell line are shown in Table 1. Sensitivity of each cell line to the EZH1/2 dual inhibitor associated with expression of EZH2 expression in each cell line (Table 1 and Figure 2B). The EZH1 highly expressing cells, such as the A204.1 and G401.6TG cells, showed low sensitivity to the EZH2-selective inhibitors (Table 1 and Figure 2B), suggesting that expression of EZH1 inversely associates with the anti-proliferative effect of EZH2-selective inhibitors.

We also tested the effect of the EZH inhibitors on *SMARCB1* wild-type rhabdomyosarcoma (RMS) cell line RD. The anti-proliferative effect was barely observed in *SMARCB1* wild-type RD cells (Figures 2A and S2C). These results suggest that the inhibitors act more selectively in *SMARCB1*-deficient cells.

In A204.1 and TTC642 cells, the EZH1/2 dual inhibitor DS-3201b reduced H3K27me3 levels more efficiently than the EZH2-selective inhibitors or partially selective inhibitors (Figure 2C). Because the knockdown of *EZH2* led to increased expression of EZH1 protein (Figure 1B), we examined whether chemical inhibition of EZH2 also increased expression of EZH1. EPZ-6438 increased EZH1 protein expression in both A204.1 and TTC642 cells (Figure 2D). Increased expression of *EZH1* mRNA was also observed in EPZ-6438-treated A204.1 cells (Figure 2E), which is consistent with the results observed after KD of *EZH2* (Figures S1C and S1D). These findings indicate that loss of EZH2 function results in increased expression of EZH1 in MRT cells, and that EZH1/2 dual inhibitors inactivate both EZH1 and EZH2 efficiently, and may be an effective treatment for MRT.

Effect of EZH1 on MRT cell growth under conditions of EZH2 inhibition

Next, we examined the role of EZH1 in MRT cells under conditions of EZH2 inhibition. A204.1 cells expressed high levels of EZH1 (Figure 2B) and exhibited low sensitivity to the EZH2-selective inhibitor (Table 1). To investigate whether EZH1 expression is related to sensitivity to EZH2 inhibitors, A204.1 cells were treated with EPZ-6438 after KD of *EZH1*. Depletion of EZH1 enhanced the anti-proliferative effect of EPZ-6438 significantly and shifted the IC_{50} value of EPZ-6438 to 1.98 nM (Figures 3A and 3B). We then overexpressed EZH1 in A204.1 and TTC642 cells using a tetracycline-inducible gene expression system (Tet-On system) and confirmed that doxycycline (Dox) induced expression of both EZH1 protein and mRNA (Figures 3C and 3D). EZH1 overexpression attenuated the anti-proliferative activity of EPZ-6438, even in susceptible TTC642 cells, whereas no significant changes in sensitivity to DS-3201b were observed (Figure 3E). Taken together, these data suggest that EZH1 compensates for the function of EZH2 and supports MRT cell growth under conditions of EZH2 inhibition, and that depletion of EZH1 increases the efficacy of EZH2 inhibition.

Molecular mechanism underlying the anti-proliferative effect of the EZH1/2 inhibitor in MRT cells

To elucidate the molecular mechanism underlying the observed growth inhibition induced by EZH inhibitors in MRT cells, we performed RNA-sequencing (RNA-seq) analysis and compared differentially expressed genes between A204.1 cells treated with DS-3201b treatment or EPZ-6438. The analysis showed that 2,043 genes were altered significantly in DS-3201b-treated cells (upregulated, 1,414; downregulated, 629), and 956 genes were in EPZ-6438-treated cells (upregulated, 802; downregulated, 154). Of these, 584 overlapped between DS-3201b- and EPZ-6438-treated cells, whereas 1,459 were altered specifically in DS-3201b-treated cells (Figure 4A). Gene enrichment analysis revealed that DS-3201b altered genes associated significantly with cell division and cell-cycle processes (Figure 4B), suggesting that DS-3201b affects the cell cycle in MRT cells.

To further investigate whether DS-3201b regulates the cell cycle in MRT cells, we analyzed cell-cycle progression in DS-3201b- or EPZ-6438-treated A204.1 cells at days 8 and 14. Although both DS-3201b and EPZ-6438 induced cell-cycle arrest at day 14, the effect was already apparent in DS-3201b-treated cells at day 8 (Figure 5A). DS-3201b increased the percentage of cells in G1 phase, which was concomitant with a decrease in the number of cells in S phase and G2/M phase. No apparent increase in the subG1 fraction was observed at day 8, but DS-3201b increased the percentage of the

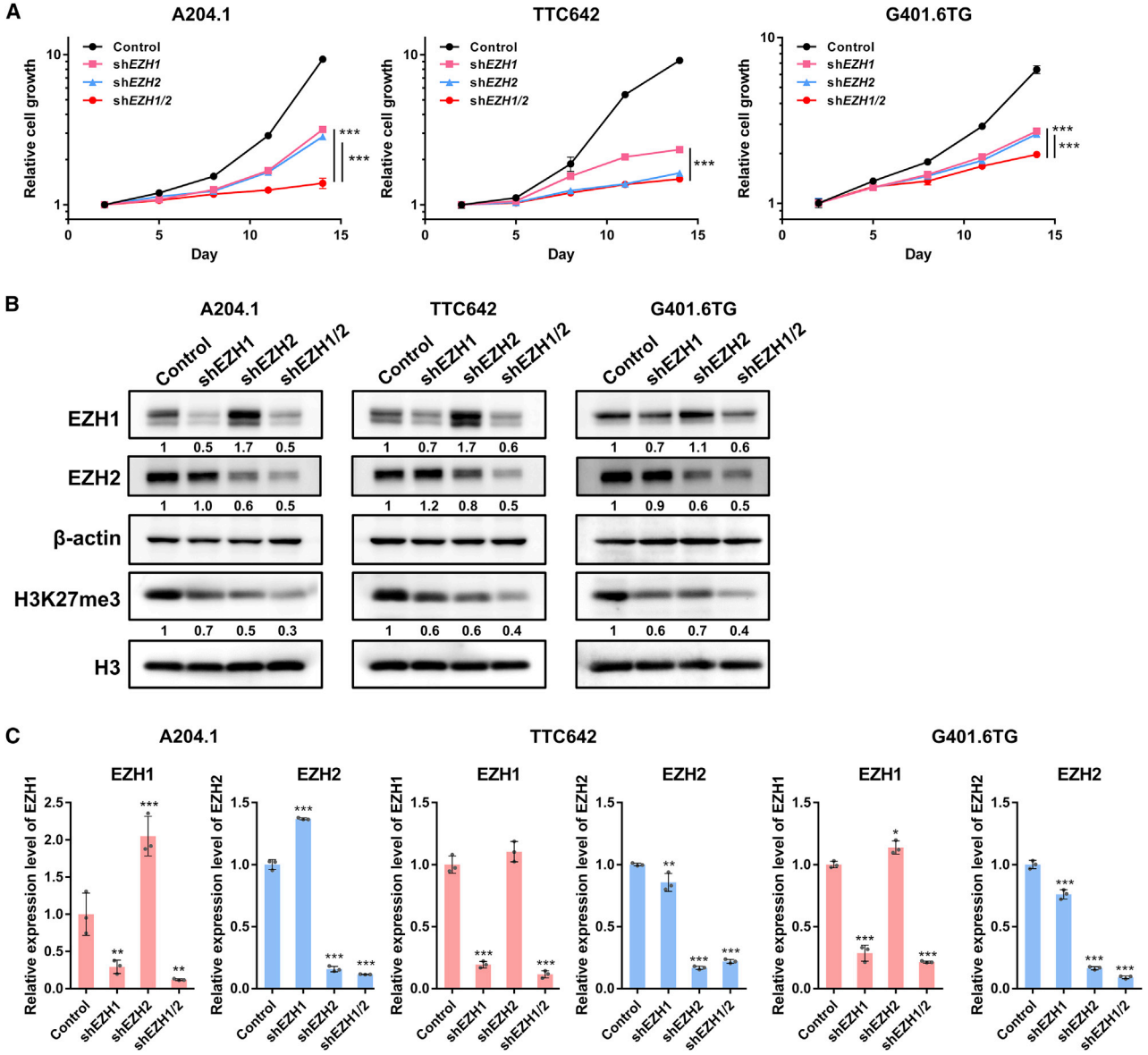

Figure 1. The function and expression of EZH1 and EZH2 in MRT

(A) The functions of EZH1 and EZH2 on cell proliferation in MRT cells. A204.1, TTC642, and G401.6TG cells were infected with retroviral sh*EZH1* and/or sh*EZH2* vectors, and transduced cells were selected with 0.5 mg/mL (A204.1) or 0.1 mg/mL (TTC642 and G401.6TG) of G418 for 7 days. The relative cell growth of the transduced cells was measured by WST-8 formazan dye (OD 450) for the indicated durations (n = 3, means ± SD). Differences were statistically evaluated by two-way ANOVA followed by Tukey's multiple comparisons test. Statistical significance between control and each KD condition (sh*EZH1*, sh*EZH2*, and sh*EZH1/2*) was observed after day 11 in all cell lines. sh*EZH1* versus control is $p < 0.0001$, sh*EZH2* versus control is $p < 0.0001$, and sh*EZH1/2* versus control is $p < 0.0001$ in all cell lines. Statistical significances between single KD and double KD on day 14 are as follows: sh*EZH1* versus sh*EZH1/2* is ***$p < 0.0001$ in all cell lines. sh*EZH2* versus sh*EZH1/2* is ***$p < 0.0001$ in A204.1 and G401.6TG cells, but $p = 0.4519$ in TTC642 cells. (B) Expression of EZH1, EZH2, and H3K27me3 proteins in cells single or double KD of *EZH1* and *EZH2*. The expression level of each protein was determined by western blotting analysis. β-actin and H3 were used as the internal controls. The numbers below EZH1, EZH2, and H3K27me3 indicate each band density relative to control (taken as "1"). (C) Expression of *EZH1* and *EZH2* mRNAs in cells single or double KD. Relative expression level of each mRNA was evaluated by qRT-PCR (n = 3, means ± SD). The expression level of the control is indicated as "1." *$p < 0.05$, **$p < 0.01$, ***$p < 0.001$ versus control. The KD efficacy was also confirmed by expression levels of proteins (B) and mRNAs (C).

subG1 fraction at day 14, suggesting that DS-3201b treatment induces apoptosis following cell-cycle arrest (Figure 5A). Gene enrichment analysis revealed apoptotic processes in the list of top 100 terms in DS-3201b-treated cells (Figure S3A). Thus, we assessed apoptosis induction by DS-3201b using Annexin V-APC and DAPI staining. We found that treatment with DS-3201b for 14 days increased the

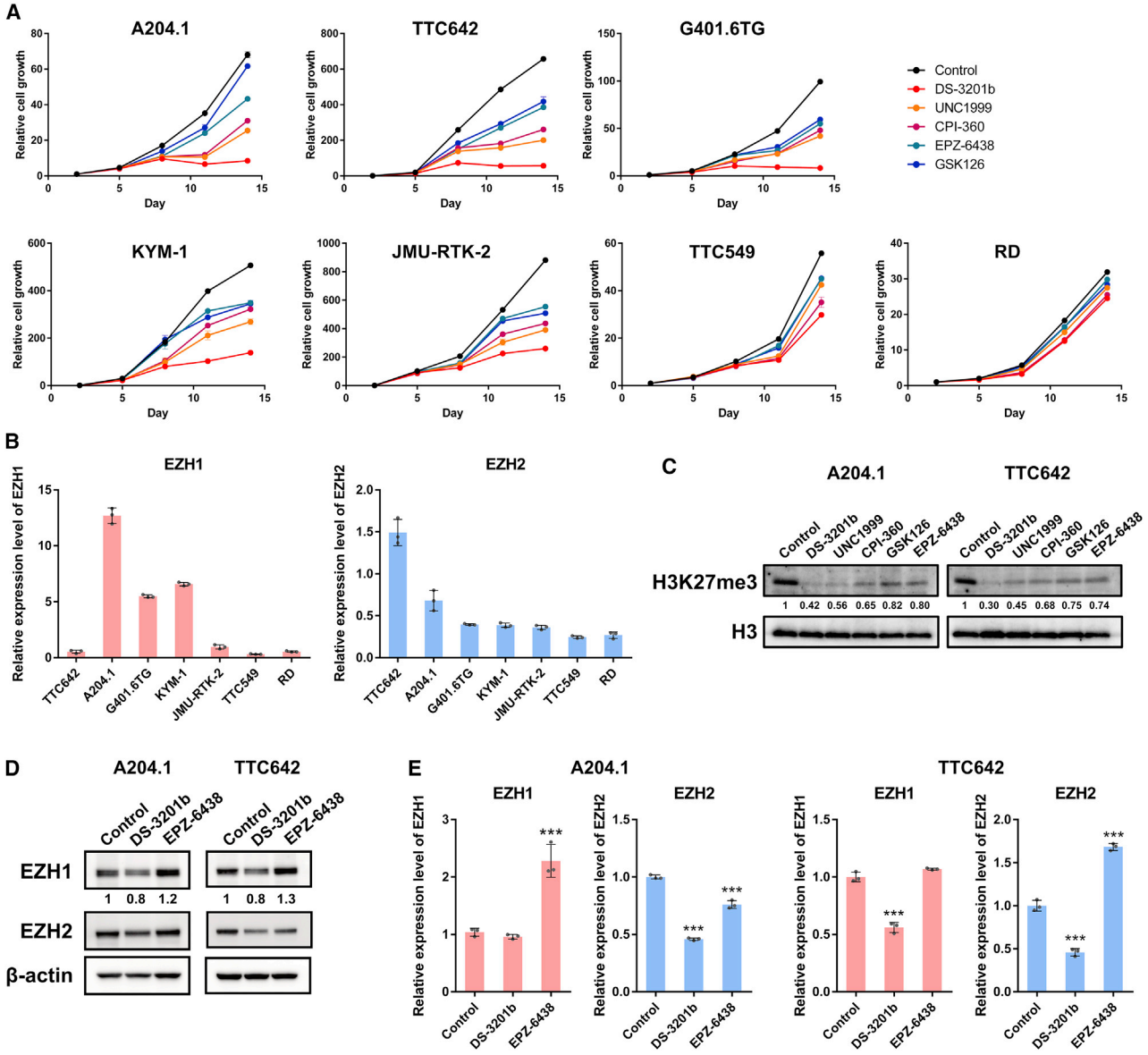

Figure 2. Dual inhibition of EZH1 and EZH2 in MRT cells

(A) The effect of EZH1/2 dual inhibitors and EZH2-selective inhibitors on the cell growth. Six MRTs (A204.1, TTC642, G401.6TG, KYM-1, JMU-RTK-2, and TTC549) and *SMARCB1* wild-type RMS (RD) cells were treated with DS-3201b, UNC1999, CPI-360, GSK126, or EPZ-6438 for the indicated durations, and relative cell growth was evaluated by a WST-8 assay (n = 3, means ± SD). Differences were statistically evaluated by two-way ANOVA followed by Tukey's multiple comparisons test. Statistical significance between control and each drug treatment (DS-3201b, UNC1999, CPI-360, GSK126, or EPZ-6438; 100 nM) is $p < 0.001$ in all MRT cell lines on day 14. (B) Relative expression levels of *EZH1* and *EZH2* mRNAs in steady state of each cell line (n = 3, means ± SD). (C) The methylation levels of H3K27 after treatment with EZH1/2 dual inhibitors and EZH2-selective inhibitors. Cells were treated with DS-3201b, UNC1999, CPI-360, GSK126, or EPZ-6438 (100 nM each) for 7 days, followed by western blotting analysis. The numbers below H3K27me3 indicate each band density relative to control (taken as "1"). (D and E) Expression of EZH1 and EZH2 proteins (D) and mRNAs (E) in DS-3201b- or EPZ-6438-treated cells. Cells were treated with DS-3201b (100 nM) or EPZ-6438 (100 nM) for 7 days, followed by western blotting and qRT-PCR, respectively. (D) The numbers below EZH1 indicate each band density relative to control (taken as "1"). (E) n = 3, means ± SD. The expression level of the control is indicated as "1." ***$p < 0.001$ versus control.

percentage of cells at the early stage of apoptosis (Figure S3B). However, another apoptotic phenotype, measured by cleavage of PARP-1 and caspase-3, was not detectable (Figure S3C), suggesting that the ratio of apoptotic cells was too low to detect signaling proteins. We speculate that the anti-proliferative activity of DS-3201b relies, at least in part, on induction of apoptosis, but that cell-cycle arrest is the most crucial molecular mechanism induced by DS-3201b in MRT cells.

Table 1. IC_{50} values of EZH inhibitors in MRT and RMS cell lines

		IC_{50} (nM, day 11)				
Cell line	Origin	DS-3201b	UNC1999	CPI-360	GSK126	EPZ-6438
TTC642	soft tissue	0.19	3.77	23.21	78.7	37.1
A204.1	soft tissue	0.47	12.3	33.9	749	399.7
G401.6TG	kidney	13.3	76.7	68.5	261.1	112.6
KYM-1	soft tissue	20.6	179.7	219.0	489.9	593.2
JMU-RTK-2	kidney	101.3	177.3	289.7	393.4	468.7
TTC549	liver	526.0	900.2	772.1	1097	1233
RD	soft tissue (RMS)	1303	2698	1442	3942	7756

Next, we sought to identify the molecule responsible for cell-cycle arrest induced by DS-3201b. Comparison of cell-cycle-associated gene expression signatures revealed that CDKN2A was markedly upregulated in DS-3201b-treated cells (Figures 5B and 5C). The qRT-PCR analysis confirmed that DS-3201b increased expression of *CDKN2A* significantly (Figure 5D). Although expression of other PRC2 target genes *CDKN2C* and *CDKN1A* was also upregulated by DS-3201b, the increase in *CDKN2A* expression was more marked and reflected the anti-proliferative effects of DS-3201b in MRT cells (Figures 5D and S4A). Double KD of *EZH1* and *EZH2* increased *CDKN2A* expression to a greater extent than single KD of either gene (Figure S4B), which correlated with the reduction of H3K27me3 levels and suppression of cell proliferation (Figures 1A and 1B). We examined the presence of the H3K27me3 marks at the *CDKN2A* locus in A204.1 cells by performing chromatin immunoprecipitation (ChIP) coupled with qPCR (ChIP-qPCR). H3K27me3 was more accumulated at the exon 1α (*p16-CDKN2A*) compared with exon 1β (*p14-ARF*). DS-3201b reduced the H3K27me3 marks at the *CDKN2A* locus significantly (Figures 5E and 5F). The reduction in H3K27me3 marks at the *CDKN2A* locus was induced significantly by single KD of *EZH1* or *EZH2*, although the decrease in H3K27me3 was more marked after double KD of *EZH1* and *EZH2* (Figure S4C). Collectively, these data indicate that EZH1/2 dual inhibition cancels H3K27me3 accumulation and effectively reactivates EZH1/2 target genes such as *CDKN2A* in MRT cells.

Morphological changes in MRT cells induced by EZH inhibitors

Gene enrichment analysis also revealed that both DS-3201b and EPZ-6438 significantly altered genes associated with cell growth, cell morphology, and differentiation (Figure 4B). EZH2 maintains the stem cell-associated signature in Smarcb1-deficient mouse embryonic fibroblasts and SMARCB1-deficient human pluripotent stem cells.[6,22] EPZ-6438 induces genes responsible for neuronal differentiation and morphological changes in MRT cells,[9] which is consistent with our RNA-seq data. Morphological alteration of A204.1 cells was observed after exposure to DS-3201b for 7 days (Figure S5A). EZH inhibitors increased the number of long, thin, spindle-shaped cells. Recent studies show that EZH2 and H3K27me3 are enriched at the loci of differentiation genes.[23] Therefore, we confirmed expression of genes reported to be involved in MRT differentiation.[9,24,25] Expression of *DOCK4* and *α-SMA* increased in both DS-3201b- and EPZ-6438-treated cells (Figure S5B). Double KD of *EZH1* and *EZH2* also led to upregulation of these genes (Figure S5C). By contrast, another differentiation-related gene, CD133,[9,25] was not detected in A204.1 or TTC642 cells (data not shown). Based on these findings, we speculate that the morphological changes mediated by DS-3201b are partly associated with differentiation.

The anti-proliferative effect of the EZH1/2 dual inhibitor *in vivo*

To confirm the effects of the EZH1/2 dual inhibitor *in vivo*, we established an A204.1 xenograft mouse model. Oral administration of DS-3201b completely inhibited tumor growth and found a significant difference in tumor size between DS-3201b-treated and untreated mice at day 18 (Figure 6A). No significant body weight loss was observed during treatment (Figure 6B). Tumor size and weight were significantly lower in treated mice than in the control group (Figures 6C and 6D). We sought to compare DS-3201b with EPZ-6438 directly; however, the experiment was not successful due to the difference in solubility and the number of doses a day. Consistent with the investigation *in vitro* (Figure 2A and Table 1), EPZ-6438 slightly inhibited tumor growth in A204.1 xenografted mice, but the difference is not statistically significant (Figures S6A and S6B). On day 21, the relative tumor volume of DS-3201b-treated mice was 0.018, but that of EPZ-6438-treated mice was 0.88 (Figure S6C). Histologic analysis by H&E staining revealed that tumor tissues from the control mice consisted of densely packed tumor cells with atypical mitotic figures, indicating abnormal cell proliferation (Figure 6E). By contrast, tumor tissues from DS-3201b-treated mice were composed of fewer and loosely distributed tumor cells, and atypical mitosis was observed much more rarely than in control mice (Figure 6E). To validate the mechanism underlying the anti-tumor effects of DS-3201b *in vivo*, we evaluated expression of H3K27me3 and CDKN2A by immunohistochemistry (IHC). Complete loss of H3K27me3 was observed in DS-3201b-treated tumors (Figure 6F). Expression of CDKN2A in tumors from the DS-3201b-treated mice increased markedly, reflecting the reduction in H3K27me3 levels (Figures 6F and 6G). These results suggest that the potent anti-tumor activity of DS-3201b *in vivo* is mediated by a reduction in H3K27me3 levels, leading to upregulation of CDKN2A expression. Collectively, our findings indicate that EZH1/2 dual inhibitors efficiently suppress tumor progression and may be promising drugs for successful treatment of MRT.

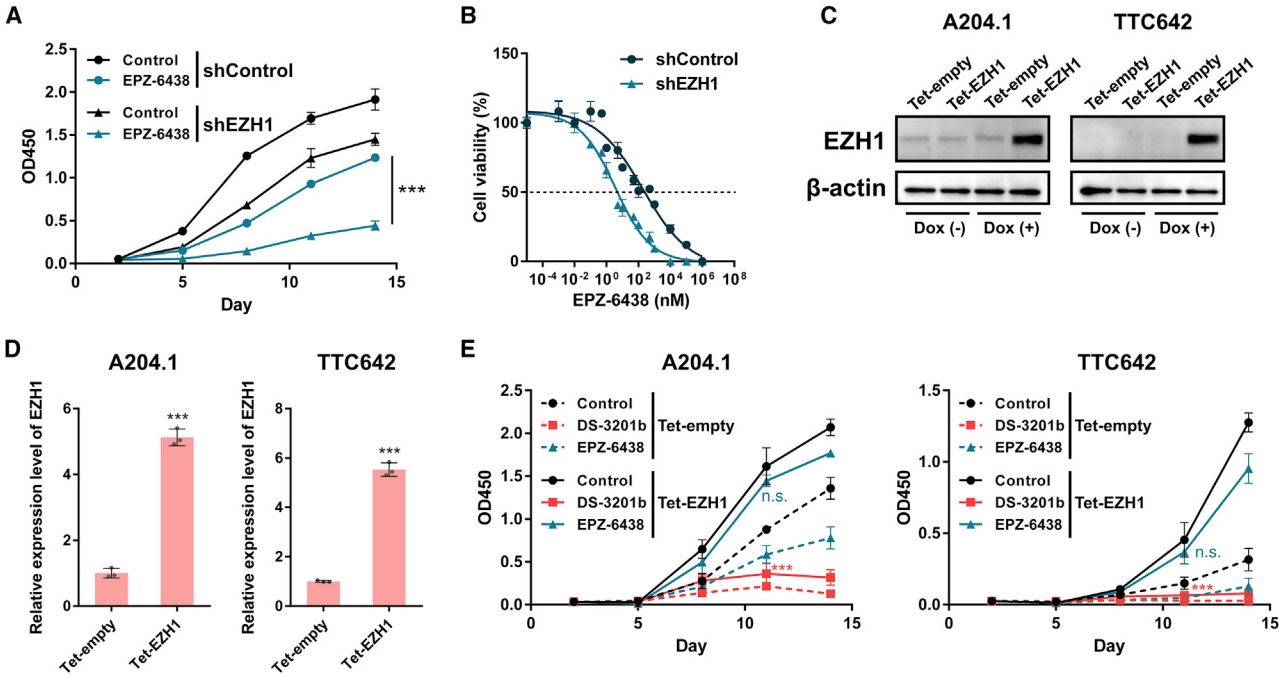

Figure 3. The function of EZH1 on MRT cell growth under the condition of EZH2 inhibition

(A) The effect of EZH1 KD under the condition of EZH2 inhibition on MRT cell growth. A204.1 cells were infected with sh*EZH1* retrovirus vector or empty vector (shControl), and transduced cells were selected with 1 μg/mL of puromycin for 10 days. The *EZH1* KD and control cells were treated with EPZ-6438 (100 nM) for the indicated durations. The relative cell growth of the cells was measured by WST-8 assay (n = 3, means ± SD). Differences were statistically evaluated by two-way ANOVA followed by Tukey's multiple comparisons test. Statistical significance between shControl and sh*EZH1* in EPZ-6438 treated cells (shControl plus EPZ-6438 versus sh*EZH1* plus EPZ-6438) is ***$p < 0.001$. (B) Dose-response curve of EZH1 KD and control cells after treatment with various doses of EPZ-6438 (n = 3, means ± SD). Dose-dependent effects on cell viability at day 11 are shown. (C–E) The overexpression of EZH1 in MRT cells. Cells were infected with retroviral Tet-EZH1 or Tet-empty (as a control) vectors, and transduced cells were selected with 5 μg/mL of blasticidin for 10 days. The cells were incubated with 1 μg/mL of doxycycline (Dox) for 5 days, and GFP^+ cells were sorted. (C) Expression of EZH1 protein in the presence or absence of Dox. (D) *EZH1* mRNA expression induced by Dox treatment (n = 3, means ± SD). The expression level of the Tet-empty is indicated as "1." ***$p < 0.001$ versus Tet-empty. (E) The effect of EZH1 overexpression on the anti-proliferative effect of EZH inhibitors. The EZH1 overexpressed cells were treated with DS-3201b (100 nM) or EPZ-6438 (100 nM) for the indicated duration, and relative cell growth was measured by a WST-8 assay (n = 3, means ± SD). Differences were statistically evaluated by two-way ANOVA followed by Tukey's multiple comparisons test. n.s., not significant, ***$p < 0.001$ versus control. DS-3201b versus control is $p < 0.0001$, and EPZ-6438 versus control is $p = 0.4448$ on day 11 in Tet-EZH1 transduced A204.1 cells. DS-3201b versus control is $p < 0.0001$, and EPZ-6438 versus control is $p = 0.4036$ on day 11 in Tet-EZH1 transduced TTC642 cells.

DISCUSSION

MRTs are rare and extremely aggressive pediatric cancers that currently have no consistently efficacious therapeutics. Mutations or deletions in the *SMARCB1* gene are observed in virtually all MRTs. Previous studies identified an antagonistic functional relationship between SWI/SNF and PRC2 complexes, and that loss of SMARCB1 results in increased expression of EZH2, widespread accumulation of H3K27me3, repression of PRC2 target genes, and tumor formation.[6,7]

In this study, we revealed that EZH1, as well as EZH2, also contributes to MRT cell growth and H3K27 methylation. We showed that both EZH1 and EZH2 are responsible for accumulation of H3K27me3 at one of the PRC2 targets, the *CDKN2A* locus. EZH1 depletion enhances the effect of EZH2 inhibition in MRT cells. These data suggest that inhibition of EZH1 efficiently reduces residual H3K27me3 after EZH2 inhibition, reactivates the PRC2 target genes, and suppresses MRT cell growth. The double KD of EZH1 and EZH2 does not induce the destabilization of the PRC2 complex, at least in the duration we examined (Figure S1E). We also demonstrated that EZH1/2 dual inhibitors markedly suppress the growth of MRT cells even more selectively in *SMARCB1*-deficient cells, consistent with EPZ-6438.[9] Several SWI/SNF complex members are genetically altered in a wide variety of cancers, suggesting that dual inhibition of EZH1/2 may be an effective treatment for these cancers.

We also found that the sensitivities of EZH2-selective inhibitors are inversely correlated with the EZH1 expression. While the biallelic inactivation of SMARCB1 induces the overexpression of EZH2,[6,7] the involvement of EZH1 expression has not been clarified. We used previously published datasets from the Gene Expression Omnibus database repository (GEO) and confirmed that expression of EZH2 was significantly higher in tumor tissues regardless of the onset sites, compared with that in corresponding normal tissues

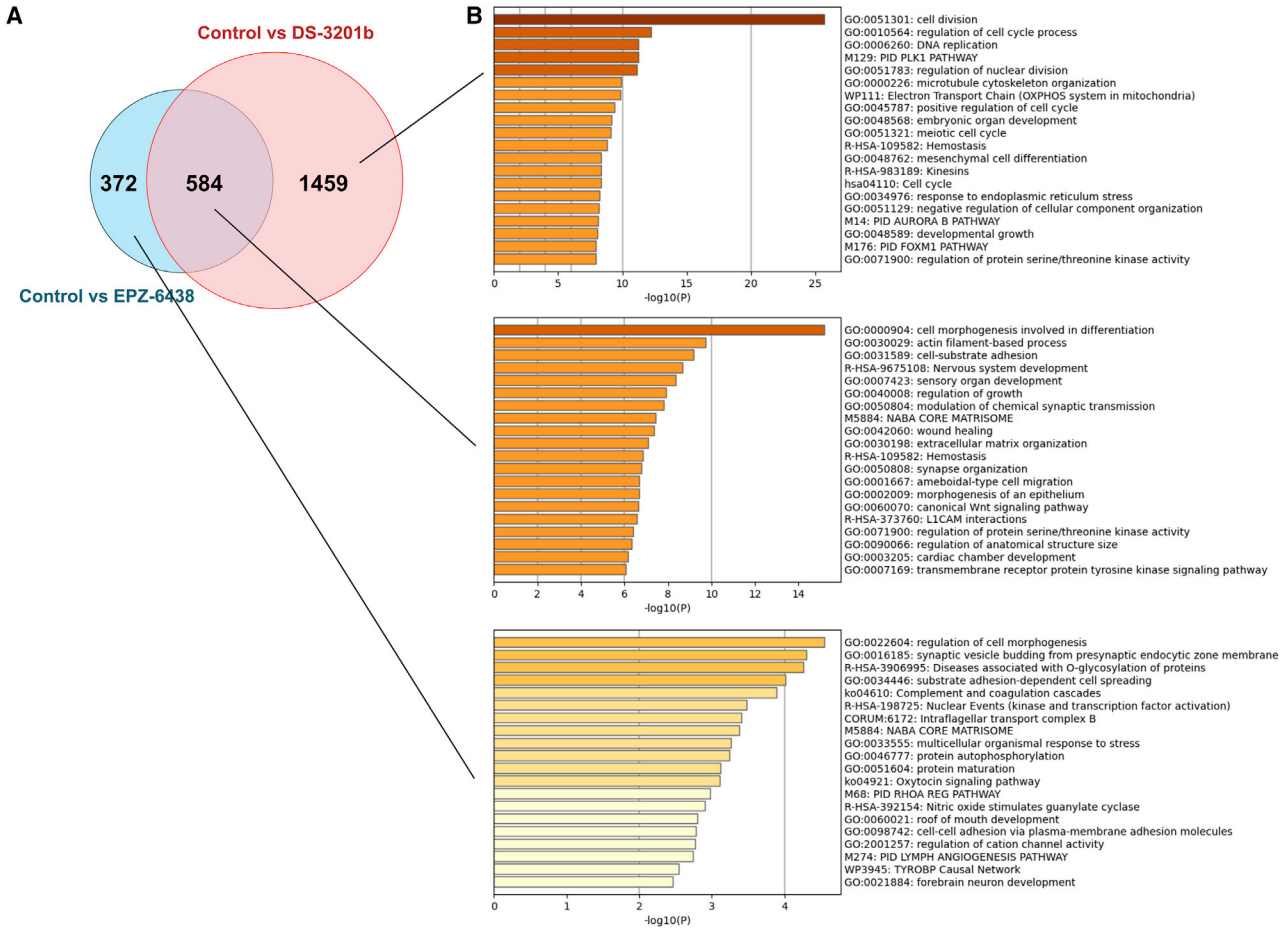

Figure 4. The molecular mechanism underlying the anti-proliferative effect of EZH inhibitors in MRT cells

(A) Venn diagram of the differentially expressed genes (false discovery rate adjusted $p < 0.05$, and fold-change > 2). A204.1 cells were treated with DS-3201b (100 nM) or EPZ-6438 (100 nM) for 14 days, followed by RNA-sequencing (RNA-seq) analysis. The number in each circle represents the number of differentially expressed genes between DS-3201b treatment and EPZ-6438 treatment. (B) The enrichment analysis of the differentially expressed genes using Metascape. Bar graphs colored by p value show the top 20 enriched terms, specifically changed by DS-3201b treatment (top), overlapped between DS-3201b and EPZ-6438 (middle), and altered by EPZ-6438 treatment (bottom).

(Figure S7A). EZH1 expression was slightly elevated in tumor tissues, but the difference was not statistically significant (Figure S7A). Exogenous expression of SMARCB1 significantly decreased the expression of EZH2 protein and mRNA (Figures S7B and S7C), leading to the growth inhibition of MRT cells (Figure S7D). EZH1 was also reduced, but only a slight change was observed in A204.1 cells (Figures S7B and S7C). EZH1 and EZH2 expressions were increased by KD of *SMARCB1* in *SMARCB1* wild-type RD cells, promoting cell growth (Figures S7E–S7H). These findings suggest that the loss of SMARCB1 upregulates both EZH1 and EZH2 expression, although SMARCB1 is only partially responsible for the expression of EZH1.

EZH1 compensates for the genetic deletion of *Ezh2* in embryonic stem cells.[14] While the enzymatic EZH2 inhibition removes EZH2 from its target loci, redeployment of EZH1 occurs at the EZH2-free loci, which prevents reduction of H3K27me3 and gene reactivation in adult T cell leukemia-lymphoma cells,[15] indicating that EZH1 has a compensatory function in response to EZH2 inhibition. In exploring the role of EZH1 in MRT cells, we discovered that the KD of *EZH2* or the selective inhibition of EZH2 increased the expression level of EZH1 protein. ChIP-qPCR analysis reveals that H3K27me3 was generally downregulated after treatment with either DS-3201b or EPZ-6438 (Figure S8), suggesting that increased expression of EZH1 is independent of the H3K27me3 reduction. Although the expression of *EZH1* mRNA differed depending on each cell line, the expression level of EZH1 protein was consistently increased in all cell lines tested. These findings suggest that transcriptional regulation may be partly involved in the increased expression of EZH1, while other conceivable hypotheses are that the protein modification pathway or translational regulation is related to the expression or

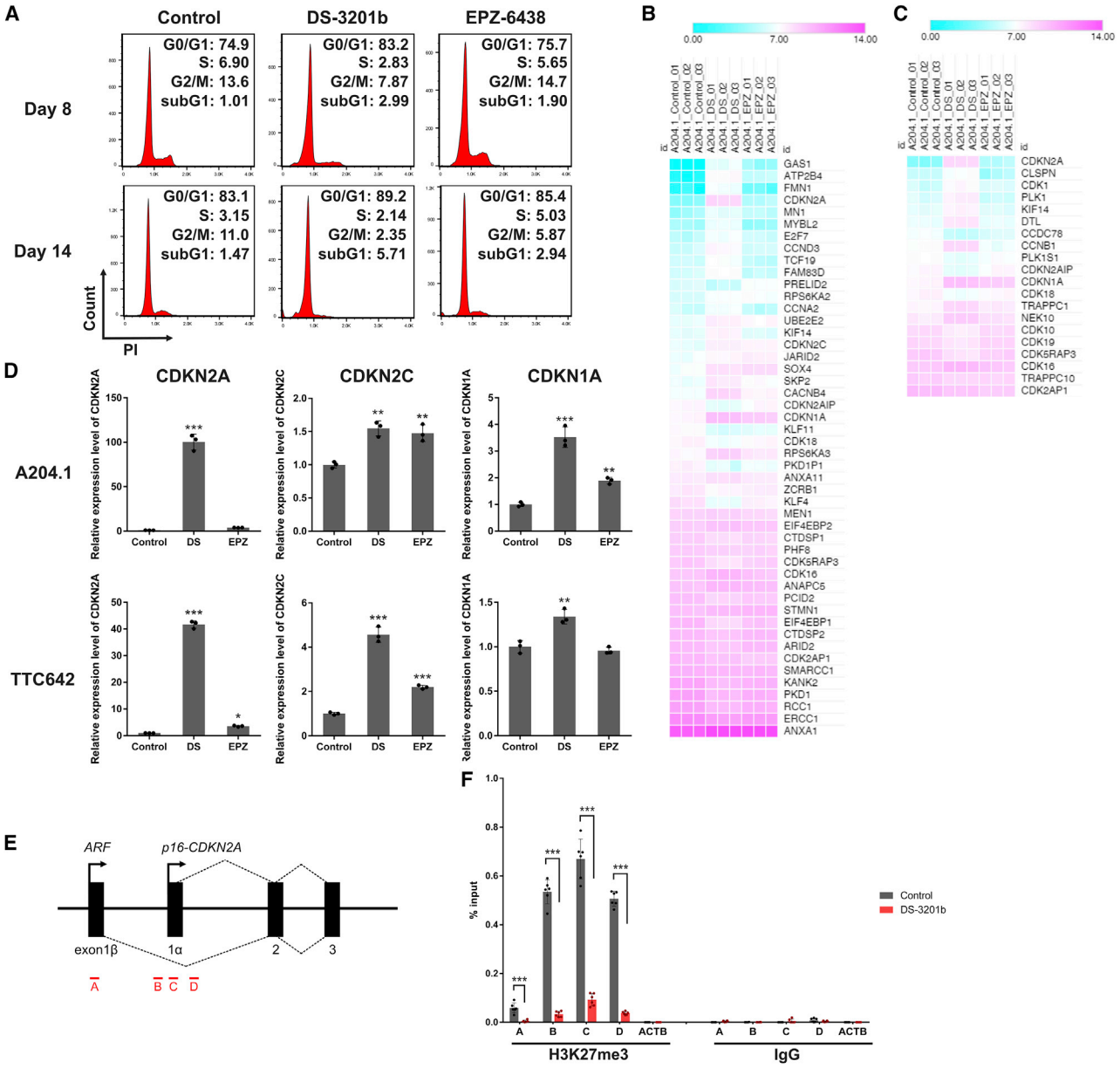

Figure 5. The reactivation of CDKN2A, one of the EZH1/2 targets, and induction of cell-cycle arrest by EZH1/2 dual inhibition

(A) Representative histograms of cell-cycle analysis. A204.1 cells were treated with DS-3201b (100 nM) or EPZ-6438 (100 nM) for the indicated duration, followed by the cell-cycle analysis with PI-staining. The y axes represent cell numbers, and x axes show DNA content (PI intensity). The numbers indicate the percentages of cells in each cell-cycle phase. (B and C) Heatmaps of differentially expressed genes belonging to the "G1/S transition of mitotic cell cycle" (GO: 0000082; B) and "G2/M transition of mitotic cell cycle" (GO: 0000086; C) terms. Mean values of signal intensity acquired from RNA-seq data are represented by colors (n = 3 each, false discovery rate adjusted $p < 0.05$, fold-change > 2). (D) Expression of *CDKN2A*, *CDKN2C*, and *CDKN1A* mRNAs in DS-3201b- or EPZ-6438-treated cells. Cells were treated with DS-3201b (DS; 100 nM) or EPZ-6438 (EPZ; 100 nM) for 7 days, followed by qRT-PCR. n = 3, means ± SD. The expression level of the control is indicated as "1." *$p < 0.05$, **$p < 0.01$, ***$p < 0.001$ versus control. (E) Schematic of the *CDKN2A* locus and the locations of primer pairs for ChIP-qPCR analysis. (F) H3K27me3 enrichment at the *CDKN2A* locus. A204.1 cells were treated with DS-3201b (100 nM) for 7 days, followed by ChIP-qPCR analysis. Normal rabbit IgG was used as a negative control for the immunoprecipitation. The primer pair against ACTB was used as a negative control for the qPCR. n = 6, means ± SD. ***$p < 0.001$, as indicated by the bracket.

stability of EZH1 protein. As shown in Figure 4B, genes associated with protein modification are specifically enriched in EPZ-6438-treated cells. Previous reports indicate that the translation of EZH2 is regulated by microRNAs (miRNAs), such as miR-101.[26] Based on the TargetScan database (http://www.targetscan.org/), the miRNAs predicted to be associated with EZH1 expression are entirely

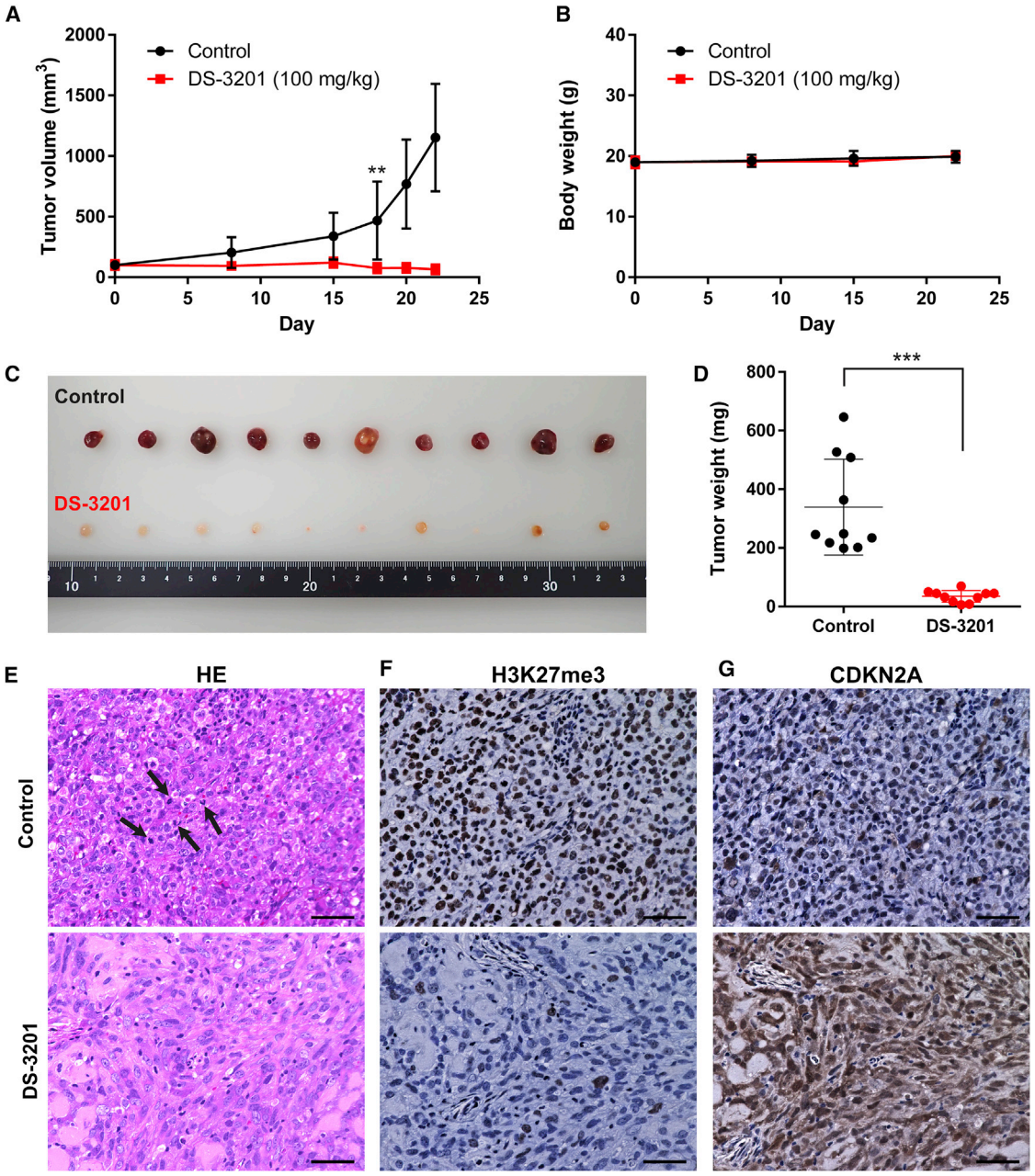

Figure 6. The anti-proliferative effect of EZH1/2 dual inhibitor *in vivo*

(A) The tumor volume of A204.1 xenograft mice. The mice were orally administered once daily with 100 mg/kg DS-3201 (calculated as a free-body DS-3201a, n = 10) or water (as control, n = 10). Differences were statistically evaluated by two-way ANOVA followed by Tukey's multiple comparisons test. DS-3201 versus control is **p = 0.003 at day 18. (B) Body weight of the A204.1 xenograft mice during the treatments. (C and D) Representative image (C) and weight (D) of tumors from all of the A204.1 xenograft mice at experimental endpoint (day 22). Differences were statistically evaluated by Mann-Whitney test. ***p < 0.001 versus control. (E) Representative images of H&E staining. The tumor tissues from the control group had a high number of mitoses (5–10 per high power field [HPF]) with abnormal mitotic figures, as shown by the arrows. DS-3201-treated tumor tissues rarely had mitosis (0–1 HPF). Scale bars, 50 μm. (F and G) Representative images of immunohistochemical staining of H3K27me3 (F) and CDKN2A (G). The tumors whose volume and weight were closest to the mean were used for immunohistochemistry. Scale bars, 50 μm.

different from those targeting EZH2. The depletion or inhibition of EZH2 may mediate the miRNAs targeting EZH1, resulting in the increased expression of EZH1 protein. Although there are several plausible mechanisms, further investigation is needed to elucidate the regulation of EZH1 expression under the condition of EZH2 depletion or inhibition.

We investigated the mode of action underlying the MRT cell growth inhibition of the EZH1/2 dual inhibitor and found that the CDKN2A-mediated cell-cycle arrest is one of the most crucial molecular mechanisms. The induction of apoptosis and cell differentiation by EZH1/2 dual inhibitors also has been reported in hematologic malignancies.[15-17] Our data reveal that DS-3201b treatment induces the morphological changes of MRT cells and increases the expression of *DOCK4* and *α-SMA*. Although these genes are reported to be involved in MRT differentiation, whether the EZH1/2 dual inhibitor induces differentiation in MRT cells cannot be concluded. As reported previously,[9] morphological alteration is not observed in all cell lines. Various genes have been proposed as differentiation markers, whereas all marker genes are not expressed in all MRT cells. MRT can arise throughout the body, and the expressions of marker genes are not necessarily reflected in a clinical case. Further study about differentiation markers of MRT may be helpful to investigate the detailed mechanism of EZH1/2 dual inhibitors.

We showed the efficacy of the EZH1/2 dual inhibitor in the xenograft mice model. Our data strongly suggest that DS-3201b effectively suppresses tumor growth without significant adverse effects. Repeated dose toxicity study also demonstrated that DS-3201b shows no critical or severe toxicity.[19] Phase I investigator-initiated study of DS-3201b in pediatric, adolescent, and young adult patients with malignant solid tumors (ELEPHANT trial, NCCH1904/MK007 trial) is now undergoing. Collectively, this study provides evidence that EZH1 and EZH2 are effective targets in MRT cells, and our findings support further studies of EZH1/2 dual inhibitors as a potential therapeutic option for patients with MRT.

MATERIALS AND METHODS

Cell culture and treatment

Human MRT cell lines A204.1, TTC642, G401.6TG, and TTC549 were described elsewhere.[27,28] The cells were cultured in RPMI-1640 medium (30264-56; Nacalai Tesque, Kyoto, Japan) supplemented with 10% heat-inactivated FBS (10270106; Thermo Fisher Scientific, Waltham, MA, USA) and 1% penicillin/streptomycin (P/S, 26253-84; Nacalai Tesque). JMU-RTK-2 (JCRB1484) was purchased from the Japanese Collection Research Bioresources Cell Bank (Osaka, Japan). JMU-RTK-2 cells were cultured in DMEM (08456-36; Nacalai Tesque) plus 10% FBS and 1% P/S. KYM-1 (JCRB0627) and human rhabdomyosarcoma cell line RD (JCRB9072) were obtained as gifts from Prof. Yukihiro Akao, Gifu University.[29] RD cells were cultured in Eagle's minimum essential medium (M4655; Merck, Darmstadt, Germany) with 10% FBS and 1% P/S, and KYM-1 cells were cultured in a 1:1 mixture of DMEM and Ham's F12 medium (17458-65; Nacalai Tesque) supplemented with 10% FBS and 1% P/S. All cell lines were maintained at 37°C with 5% CO_2. The cells were tested for mycoplasma contamination using an e-Myco Plus Mycoplasma PCR Detection Kit (25,237; iNtRON Biotechnology, Burlington, MA, USA).

For *in vitro* experiments, an EZH1/2 dual inhibitor, DS-3201b (also called valemetostat, HY-109108A; MedChemExpress, Monmouth Junction, NJ, USA), partially selective inhibitors, UNC1999 (S7165; Selleck, Houston, TX, USA), and CPI-360 (S7656; Selleck), and EZH2-selective inhibitors, GSK126 (S7061; Selleck), and EPZ-6438 (namely tazemetostat, E7438; Selleck) were dissolved in DMSO and added to the cell culture medium at a final concentration of DMSO <0.1%; this concentration showed no significant effect on the growth and differentiation of the cells (data not shown). The relative cell growth was measured by the absorption spectrum of WST-8 formazan dye (OD 450). The detailed information of the cell growth assay is shown in the supplemental methods.

Protein extraction and western blotting

Whole cell lysate preparations and western blotting experiments were carried out as described previously.[30] Histone proteins were isolated by the acid extraction method.[31] The primary antibodies used for western blotting are listed in the supplemental methods.

RNA isolation and RT-PCR

Total RNA was isolated from cells by using a NucleoSpin RNA Plus kit (740984; Takara, Otsu, Japan) according to the manufacturer's protocol. To synthesize cDNA, total RNA was reverse transcribed with SuperScript IV VILO (11766050; Invitrogen, Carlsbad, CA, USA). Quantitative PCR was then performed using real-time PCR system (QuantStudio 12K Flex; Applied Biosystems, Waltham, MA, USA) with Taqman probes (Applied Biosystems) or specific primers and SYBRGreen (Roche). The probes and primers used in this study are summarized in the supplemental methods.

In vivo xenograft studies

BALB/c *nu/nu* nude mice were obtained from Japan SLC (Hamamatsu, Japan). After 1 week of preliminary care, mice were used for experiments. Human MRT A204.1 cells (2×10^6 cells) were suspended in 100 μL of 50% Matrigel (#356234; Corning, NY, USA) prepared in PBS and subcutaneously inoculated into the left flank of 5-week-old female mice. After the mean tumor volume had reached approximately 100 mm^3, the mice were randomized and separated into two groups. The grouping day was set as day 0, and treatment was started at day 1. DS-3201b (valemetostat tosylate) was suspended in the sterile purified water and administered orally once daily at a dose of 100 mg/kg (calculated as a free-body DS-3201a). EPZ-6438 was suspended in 5% DMSO, 40% PEG300, 5% Tween 80, and 50% sterile purified water. Tumor size was monitored by measuring the length (L) and width (W), and the volumes (V) were estimated according to the following formula: $V = (L \times W^2) \times 0.5$. The day after the final administration, the mice were killed for the assessment of tumor tissues.

Statistical analysis

Each experiment was performed in triplicate. Data are presented as the mean ± SD. Unless stated otherwise, differences were statistically evaluated by one-way ANOVA followed by the t test or Dunnett's multiple comparison test. Statistic evaluation was performed using GraphPad 6.0 (GraphPad Software, La Jolla, CA, USA) and JMP 14

(SAS Institute, Cary, NC, USA) software. The level of significance was set at $p < 0.05$.

Study approval

All animal experimental protocols were approved by the Institutional Animal Care and Use Committee at the National Cancer Center. Animal experiments were conducted in accordance with the Guidelines for the Care and Use of Laboratory Animals. Each experiment was carried out in a specific pathogen-free environment at the animal facility of the National Cancer Center, in accordance with institutional guidelines.

DATA AVAILABILITY

The gene expression data generated during this study are deposited in GEO with accession numbers GSE205086.

SUPPLEMENTAL INFORMATION

Supplemental information can be found online at https://doi.org/10.1016/j.omto.2022.09.006.

ACKNOWLEDGMENTS

The authors thank Yukihiro Akao for providing the cell lines. We are grateful to Kazuki Heishima for providing expert advice and for histology. This work was supported by the National Cancer Center Research and Development Fund (2020-S-6 to H.S.) and the Rare Cancer Grant II in the National Cancer Center Japan (G018 to H.S.).

AUTHOR CONTRIBUTIONS

H.S. designed the study and performed most of the experiments, and data collection and analysis, as well as writing and final approval of the manuscript. R.S., M.N., A.H., K.Y., K.T., J.I., Y.K., T.O., and C.O. provided technical support for experiments and approved the final version of the manuscript. I.K. helped to design the experiments, helped to write the manuscript, and assisted with final approval of the manuscript.

DECLARATION OF INTERESTS

I.K. received research grants from Daiichi Sankyo Company (CH24043) and Sumitomo Dainippon Pharma (C2018-189).

REFERENCES

1. Biegel, J.A., Tan, L., Zhang, F., Wainwright, L., Russo, P., and Rorke, L.B. (2002). Alterations of the hSNF5/INI1 gene in central nervous system atypical teratoid/rhabdoid tumors and renal and extrarenal rhabdoid tumors. Clin. Cancer Res. *8*, 3461–3467.
2. Dufour, C., Beaugrand, A., Le Deley, M.C., Bourdeaut, F., André, N., Leblond, P., Bertozzi, A.I., Frappaz, D., Rialland, X., Fouyssac, F., et al. (2012). Clinicopathologic prognostic factors in childhood atypical teratoid and rhabdoid tumor of the central nervous system: a multicenter study. Cancer *118*, 3812–3821.
3. Farber, B.A., Shukla, N., Lim, I.I.P., Murphy, J.M., and La Quaglia, M.P. (2017). Prognostic factors and survival in non-central nervous system rhabdoid tumors. J. Pediatr. Surg. *52*, 373–376.
4. Cheng, H., Yang, S., Cai, S., Ma, X., Qin, H., Zhang, W., Fu, L., Zeng, Q., Wen, M., Peng, X., et al. (2019). Clinical and prognostic characteristics of 53 cases of extracranial malignant rhabdoid tumor in children. A single-institute experience from 2007 to 2017. Oncologist *24*, e551–e558.
5. Versteege, I., Sévenet, N., Lange, J., Rousseau-Merck, M.F., Ambros, P., Handgretinger, R., Aurias, A., and Delattre, O. (1998). Truncating mutations of hSNF5/INI1 in aggressive paediatric cancer. Nature *394*, 203–206.
6. Wilson, B.G., Wang, X., Shen, X., McKenna, E.S., Lemieux, M.E., Cho, Y.J., Koellhoffer, E.C., Pomeroy, S.L., Orkin, S.H., and Roberts, C.W. (2010). Epigenetic antagonism between polycomb and SWI/SNF complexes during oncogenic transformation. Cancer Cell *18*, 316–328.
7. Helming, K.C., Wang, X., and Roberts, C.W.M. (2014). Vulnerabilities of mutant SWI/SNF complexes in cancer. Cancer Cell *26*, 309–317.
8. Margueron, R., and Reinberg, D. (2011). The Polycomb complex PRC2 and its mark in life. Nature *469*, 343–349.
9. Knutson, S.K., Warholic, N.M., Wigle, T.J., Klaus, C.R., Allain, C.J., Raimondi, A., Porter Scott, M., Chesworth, R., Moyer, M.P., Copeland, R.A., et al. (2013). Durable tumor regression in genetically altered malignant rhabdoid tumors by inhibition of methyltransferase EZH2. Proc. Natl. Acad. Sci. USA *110*, 7922–7927.
10. Kurmasheva, R.T., Sammons, M., Favours, E., Wu, J., Kurmashev, D., Cosmopoulos, K., Keilhack, H., Klaus, C.R., Houghton, P.J., and Smith, M.A. (2017). Initial testing (stage 1) of tazemetostat (EPZ-6438), a novel EZH2 inhibitor, by the Pediatric Preclinical Testing Program. Pediatr. Blood Cancer *64*.
11. Torchia, J., Golbourn, B., Feng, S., Ho, K.C., Sin-Chan, P., Vasiljevic, A., Norman, J.D., Guilhamon, P., Garzia, L., Agamez, N.R., et al. (2016). Integrated (epi)-genomic analyses identify subgroup-specific therapeutic targets in CNS rhabdoid tumors. Cancer Cell *30*, 891–908.
12. Kim, K.H., and Roberts, C.W. (2016). Targeting EZH2 in cancer. Nat. Med. *22*, 128–134.
13. Italiano, A., Soria, J.C., Toulmonde, M., Michot, J.M., Lucchesi, C., Varga, A., Coindre, J.M., Blakemore, S.J., Clawson, A., Suttle, B., et al. (2018). Tazemetostat, an EZH2 inhibitor, in relapsed or refractory B-cell non-Hodgkin lymphoma and advanced solid tumours: a first-in-human, open-label, phase 1 study. Lancet Oncol. *19*, 649–659.
14. Shen, X., Liu, Y., Hsu, Y.J., Fujiwara, Y., Kim, J., Mao, X., Yuan, G.C., and Orkin, S.H. (2008). EZH1 mediates methylation on histone H3 lysine 27 and complements EZH2 in maintaining stem cell identity and executing pluripotency. Mol. Cell *32*, 491–502.
15. Yamagishi, M., Hori, M., Fujikawa, D., Ohsugi, T., Honma, D., Adachi, N., Katano, H., Hishima, T., Kobayashi, S., Nakano, K., et al. (2019). Targeting excessive EZH1 and EZH2 activities for abnormal histone methylation and transcription network in malignant lymphomas. Cell Rep. *29*, 2321–2337.e7.
16. Fujita, S., Honma, D., Adachi, N., Araki, K., Takamatsu, E., Katsumoto, T., Yamagata, K., Akashi, K., Aoyama, K., Iwama, A., et al. (2018). Dual inhibition of EZH1/2 breaks the quiescence of leukemia stem cells in acute myeloid leukemia. Leukemia *32*, 855–864.
17. Nakagawa, M., Fujita, S., Katsumoto, T., Yamagata, K., Ogawara, Y., Hattori, A., Kagiyama, Y., Honma, D., Araki, K., Inoue, T., et al. (2019). Dual inhibition of enhancer of zeste homolog 1/2 overactivates WNT signaling to deplete cancer stem cells in multiple myeloma. Cancer Sci. *110*, 194–208.
18. Xu, B., On, D.M., Ma, A., Parton, T., Konze, K.D., Pattenden, S.G., Allison, D.F., Cai, L., Rockowitz, S., Liu, S., et al. (2015). Selective inhibition of EZH2 and EZH1 enzymatic activity by a small molecule suppresses MLL-rearranged leukemia. Blood *125*, 346–357.
19. Honma, D., Kanno, O., Watanabe, J., Kinoshita, J., Hirasawa, M., Nosaka, E., Shiroishi, M., Takizawa, T., Yasumatsu, I., Horiuchi, T., et al. (2017). Novel orally bioavailable EZH1/2 dual inhibitors with greater antitumor efficacy than an EZH2 selective inhibitor. Cancer Sci. *108*, 2069–2078.
20. Bradley, W.D., Arora, S., Busby, J., Balasubramanian, S., Gehling, V.S., Nasveschuk, C.G., Vaswani, R.G., Yuan, C.C., Hatton, C., Zhao, F., et al. (2014). EZH2 inhibitor efficacy in non-Hodgkin's lymphoma does not require suppression of H3K27 monomethylation. Chem. Biol. *21*, 1463–1475.
21. McCabe, M.T., Ott, H.M., Ganji, G., Korenchuk, S., Thompson, C., Van Aller, G.S., Liu, Y., Graves, A.P., Della Pietra, A., 3rd, Diaz, E., et al. (2012). EZH2 inhibition as a therapeutic strategy for lymphoma with EZH2-activating mutations. Nature *492*, 108–112.
22. Terada, Y., Jo, N., Arakawa, Y., Sakakura, M., Yamada, Y., Ukai, T., Kabata, M., Mitsunaga, K., Mineharu, Y., Ohta, S., et al. (2019). Human pluripotent stem

cell-derived tumor model uncovers the embryonic stem cell signature as a key driver in atypical teratoid/rhabdoid tumor. Cell Rep. *26*, 2608–2621.e6.

23. Erkek, S., Johann, P.D., Finetti, M.A., Drosos, Y., Chou, H.C., Zapatka, M., Sturm, D., Jones, D.T.W., Korshunov, A., Rhyzova, M., et al. (2019). Comprehensive analysis of chromatin states in atypical teratoid/rhabdoid tumor identifies diverging roles for SWI/SNF and polycomb in gene regulation. Cancer Cell *35*, 95–110.e8.

24. Kato, H., Ohta, S., Koshida, S., Narita, T., Taga, T., Takeuchi, Y., and Sugita, K. (2003). Expression of pericyte, mesangium and muscle markers in malignant rhabdoid tumor cell lines: differentiation-induction using 5-azacytidine. Cancer Sci. *94*, 1059–1065.

25. Gadd, S., Sredni, S.T., Huang, C.C., and Perlman, E.J. (2010). Rhabdoid tumor: gene expression clues to pathogenesis and potential therapeutic targets. Lab. Invest. *90*, 724–738.

26. Cao, P., Deng, Z., Wan, M., Huang, W., Cramer, S.D., Xu, J., Lei, M., and Sui, G. (2010). MicroRNA-101 negatively regulates Ezh2 and its expression is modulated by androgen receptor and HIF-1alpha/HIF-1beta. Mol. Cancer *9*, 108.

27. Kuwahara, Y., Charboneau, A., Knudsen, E.S., and Weissman, B.E. (2010). Reexpression of hSNF5 in malignant rhabdoid tumor cell lines causes cell cycle arrest through a p21(CIP1/WAF1)-dependent mechanism. Cancer Res. *70*, 1854–1865.

28. Kuwahara, Y., Wei, D., Durand, J., and Weissman, B.E. (2013). SNF5 reexpression in malignant rhabdoid tumors regulates transcription of target genes by recruitment of SWI/SNF complexes and RNAPII to the transcription start site of their promoters. Mol. Cancer Res. *11*, 251–260.

29. Sugito, N., Taniguchi, K., Kuranaga, Y., Ohishi, M., Soga, T., Ito, Y., Miyachi, M., Kikuchi, K., Hosoi, H., and Akao, Y. (2017). Cancer-specific energy metabolism in rhabdomyosarcoma cells is regulated by MicroRNA. Nucleic Acid Ther. *27*, 365–377.

30. Shinohara, H., Kumazaki, M., Minami, Y., Ito, Y., Sugito, N., Kuranaga, Y., Taniguchi, K., Yamada, N., Otsuki, Y., Naoe, T., et al. (2016). Perturbation of energy metabolism by fatty-acid derivative AIC-47 and imatinib in BCR-ABL-harboring leukemic cells. Cancer Lett. *371*, 1–11.

31. Shechter, D., Dormann, H.L., Allis, C.D., and Hake, S.B. (2007). Extraction, purification and analysis of histones. Nat. Protoc. *2*, 1445–1457.

OMTO, Volume *27*

Supplemental information

Dual targeting of EZH1 and EZH2

for the treatment of malignant rhabdoid tumors

Haruka Shinohara, Rie Sawado, Makoto Nakagawa, Ayuna Hattori, Kazutsune Yamagata, Kimiharu Tauchi, Jumpei Ito, Yasumichi Kuwahara, Tsukasa Okuda, Chitose Ogawa, and Issay Kitabayashi

Figure S1

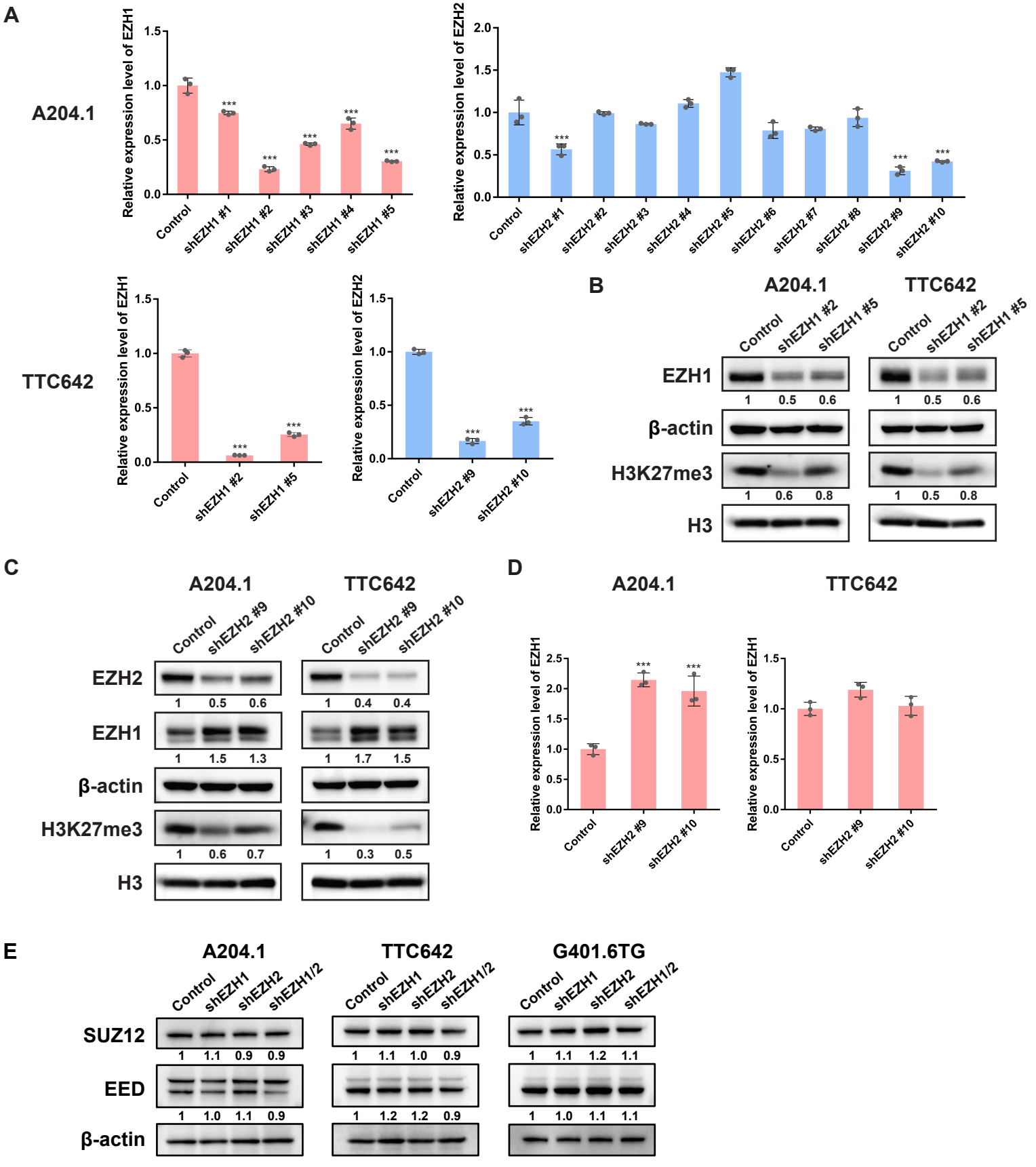

Figure S1. Effect of EZH1 and EZH2 deficiency on H3K27 methylation and EZH1 expression.

(A) Expression of *EZH1* and *EZH2* mRNAs. Cells were infected with retroviral sh*EZH1* or sh*EZH2* vectors. Next, transduced cells were selected by culturing for 3 days with 1 μg/ml of puromycin. To confirm knockdown (KD) efficacy and determine short hairpin RNA (shRNA) sequences, the relative expression level of each mRNA was evaluated by qRT-PCR (n = 3, mean ± SD). The expression level of the Control is indicated as "1". ***p < 0.001 *vs.* Control. **(B and C)** Expression of the EZH1, EZH2, and H3K27me3 proteins in *EZH1* **(B)** or *EZH2* **(C)** knockdown (KD) cells. The expression level of each protein was determined by western blotting analysis. β-actin and H3 were used as internal controls. The numbers below EZH1, EZH2, and H3K27me3 indicate the band density relative to Control (taken as "1"). The sequences of sh*EZH1* #2 and sh*EZH2* #9 were picked up for further experiments in Figure 1. **(D)** Expression of *EZH1* mRNA in *EZH2* KD cells (n = 3, means ± SD). The expression level of the Control is indicated as "1". ***p < 0.001 *vs.* Control. **(E)** Expression of SUZ12 and EED proteins in cells single or double KD of EZH1 and EZH2. The expression level of each protein was determined by Western blotting analysis. β-actin was used as the internal controls. The numbers below SUZ12 and EED indicate each band density relative to Control (taken as "1").

Figure S2

A

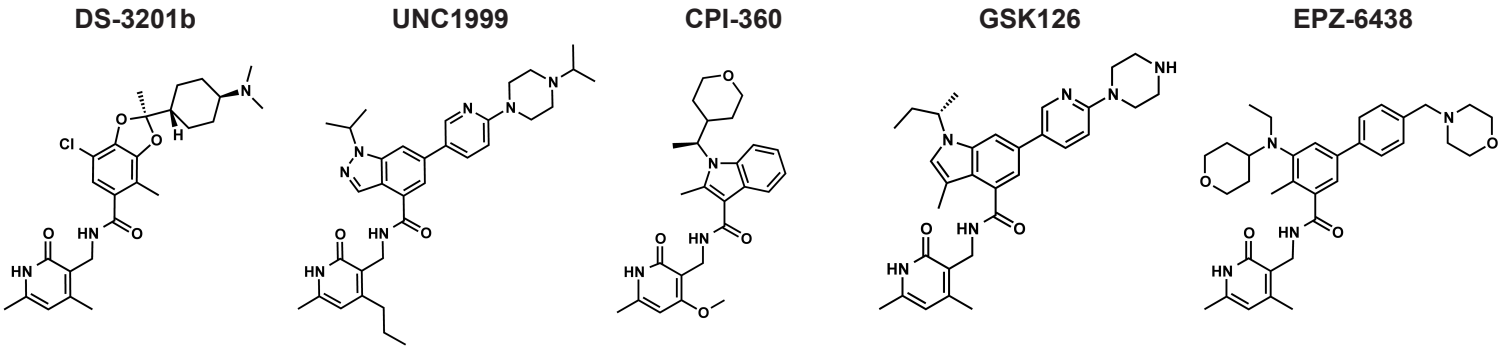

B

target	DS-3201b	UNC1999	CPI-360	GSK126	EPZ-6438
EZH1	8.4	45	102.3	680	392
EZH2	2.5	< 10	0.50	9.9	11

C

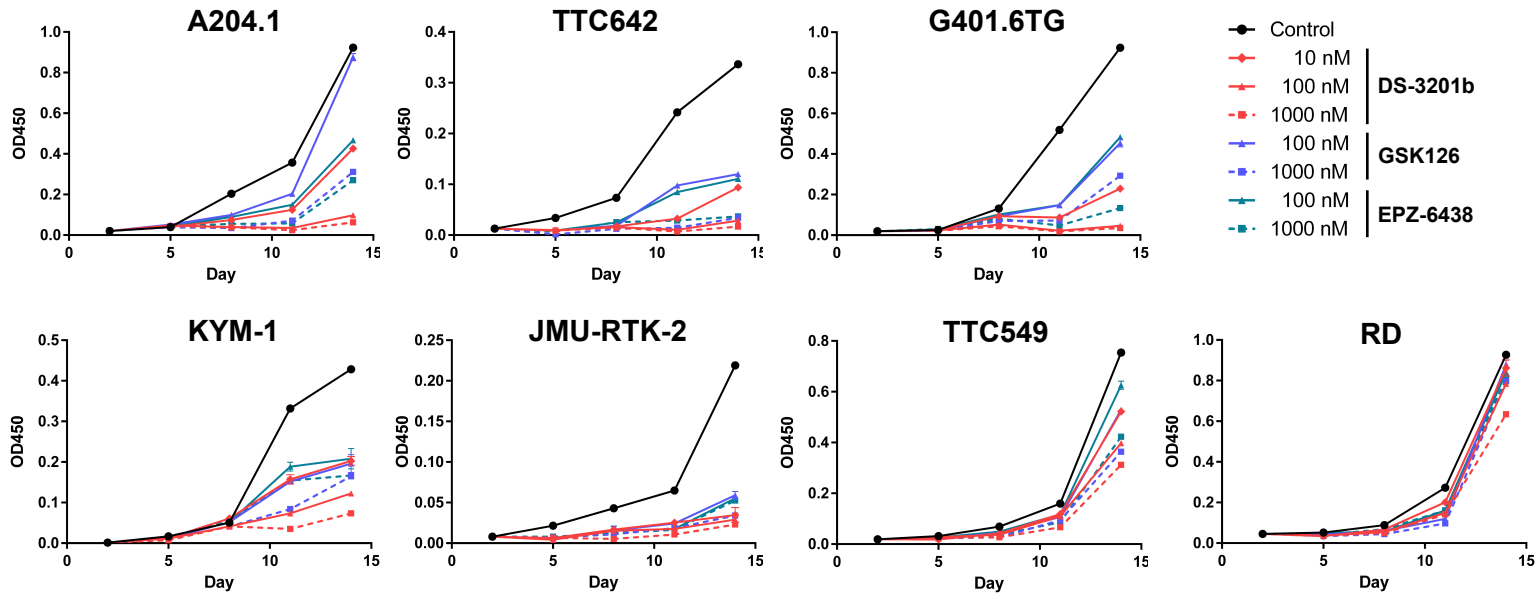

Figure S2. Characteristics of EZH inhibitors.

(A) Chemical structures of EZH inhibitors. **(B)** Officially released *in vitro* IC_{50} values of EZH inhibitors against EZH1 and EZH2. **(C)** The effect of an EZH1/2 dual inhibitor and EZH2-selective inhibitors on the cell growth. 6 MRTs (A204.1, TTC642, G401.6TG, KYM-1, JMU-RTK-2, and TTC549) and *SMARCB1*-wild type RMS (RD) cells were treated with different concentrations of DS-3201b, GSK126, or EPZ-6438 for the indicated durations, and relative cell growth was evaluated by a WST-8 assay (n = 3, means ± SD). Differences were statistically evaluated by two-way ANOVA followed by Tukey's multiple comparisons test. Statistical significance between control and each drug treatment (DS-3201b, GSK126, or EPZ-6438) is $p < 0.001$ in all cell lines. Statistical significance between DS-3201b and each EZH2 inhibitor (GSK126 or EPZ-6438) at the same concentration was observed on day 14 in all cell lines.

Figure S3

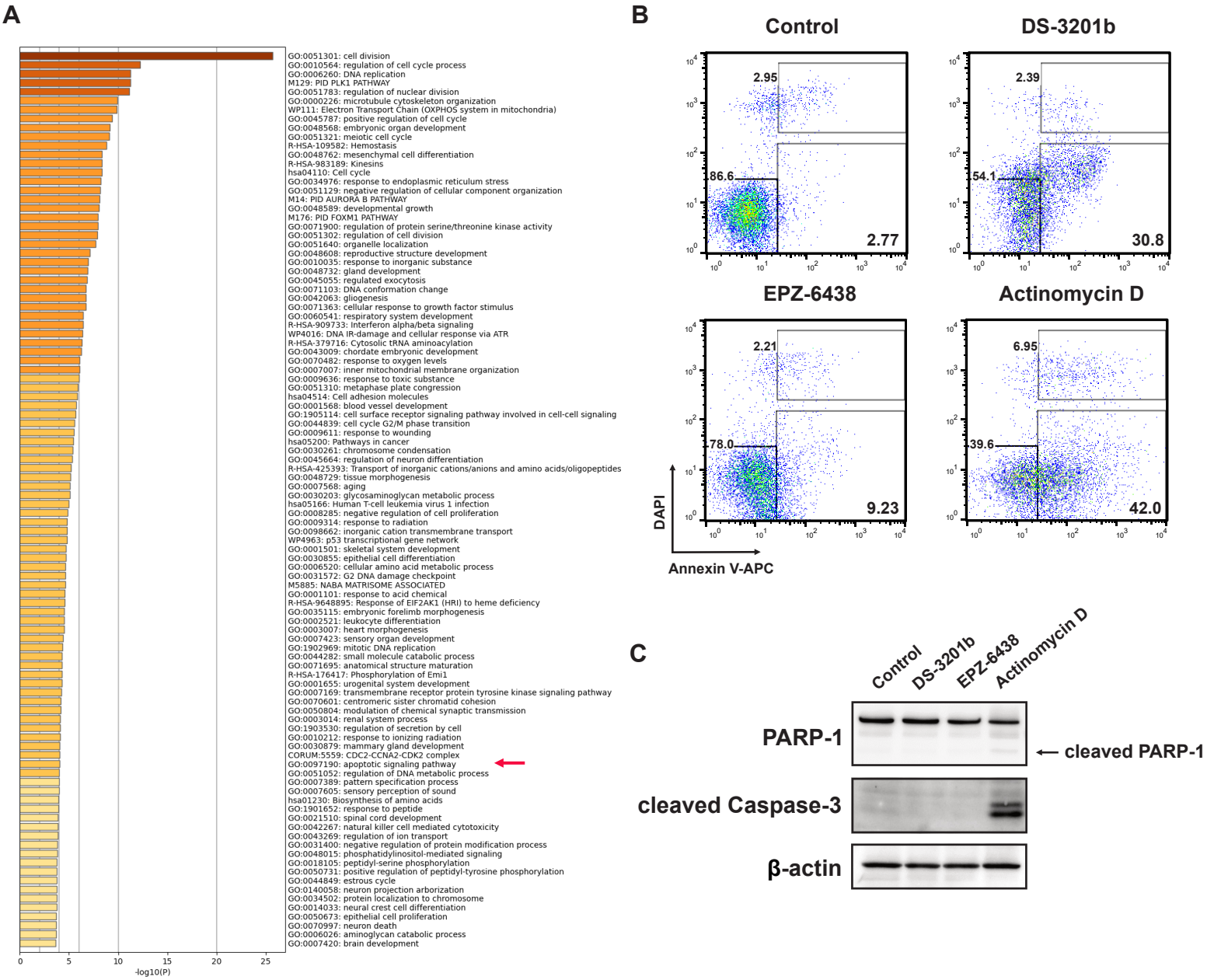

Figure S3. Apoptosis analysis of EZH inhibitor-treated cells.

(A) Enrichment analysis of differentially expressed genes (FDR-adjusted $p < 0.05$; fold change > 2) using Metascape. A204.1 cells were treated with DS-3201b (100 nM) for 14 days, followed by RNA-sequencing (RNA-seq) analysis. Bar graph colored by *p*-value shows the top 100 enriched terms altered by DS-3201b treatment. The term “apoptotic signaling pathway” (GO: 0097190) is indicated by a red arrow.

(B) Representative images of apoptosis analysis. A204.1 cells were treated with DS-3201b (100 nM) or EPZ-6438 (100 nM) for 14 days, followed by apoptosis analysis using Annexin V-APC and DAPI. Actinomycin D (1 mg/ml for 2 days) was used as a positive control. Cells in the early stage of apoptosis are presented in the lower right quadrants (Annexin V-APC-positive and DAPI-negative). The numbers in the dot plots indicate the percentage of cells in the respective quadrants. **(C)** Assessment of PARP-1 and caspase-3 cleavage in DS-3201b-, EPZ-6438-, and actinomycin D-treated cells. A204.1 cells were exposed to DS-3201b (100 nM) or EPZ-6438 (100 nM) for 14 days, or to actinomycin D (1 mg/ml) for 2 days, followed by western blotting.

Figure S4

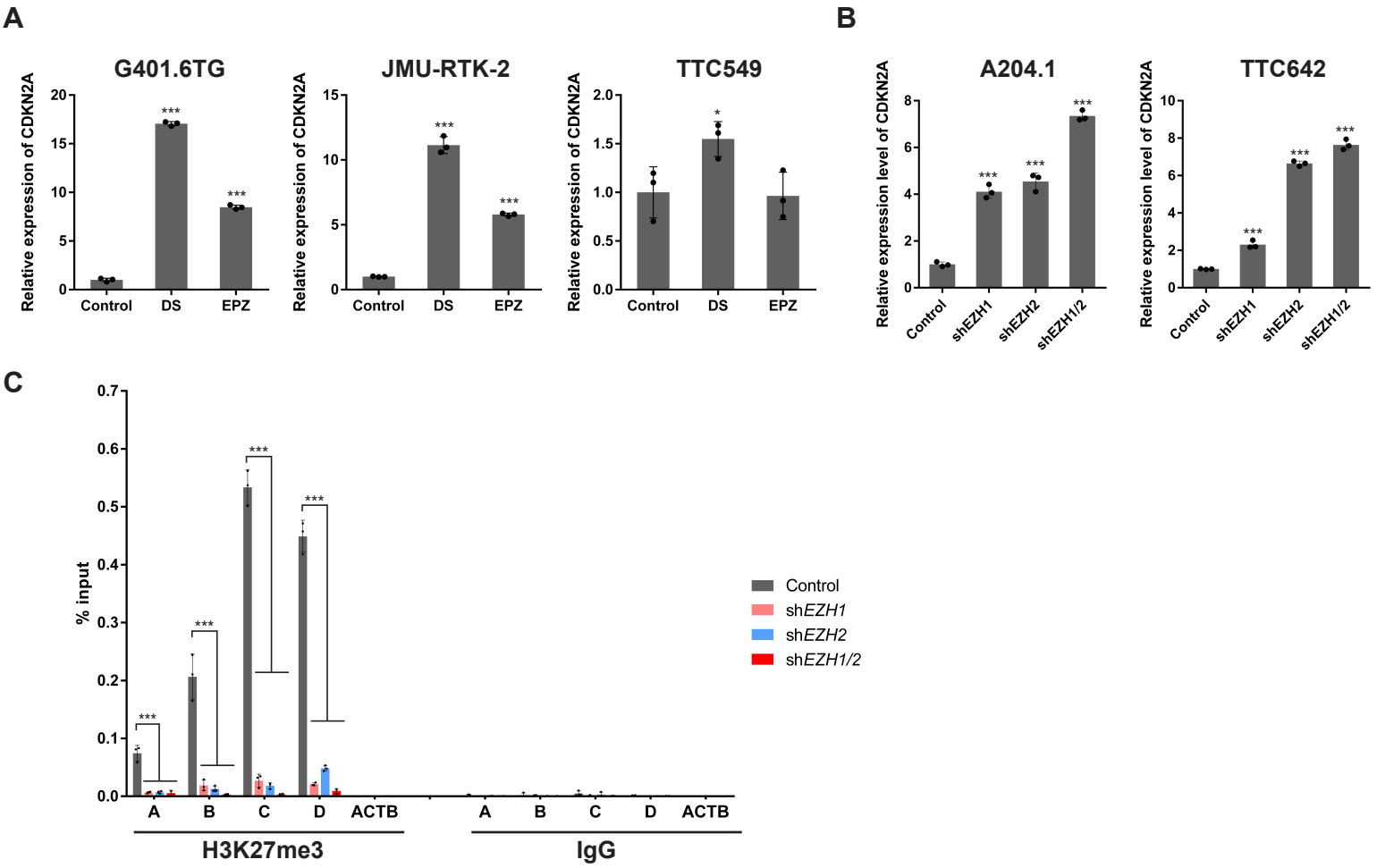

Figure S4. Upregulation of CDKN2A after EZH1/2 inhibition and depletion.

(A) Expression of *CDKN2A* mRNA in DS-3201b- or EPZ-6438-treated cells. Cells were treated with DS-3201b (DS; 100 nM) or EPZ-6438 (EPZ; 100 nM) for 7 days, followed by qRT-PCR (n = 3, means ± SD). The expression level of the Control is indicated as "1". *p < 0.05, **p < 0.01, ***p < 0.001 *vs.* Control. **(B)** Expression of *CDKN2A* mRNA in cells in which *EZH1* or *EZH2*, or both, were knocked down (n = 3; mean ± SD). The expression level of the Control is indicated as "1". ***p < 0.001 *vs.* Control. **(C)** H3K27me3 enrichment at the *CDKN2A* locus in cells in which *EZH1* or *EZH2*, or both, were knocked down. ChIP-qPCR analysis was performed using the primer pairs described in Figure 5E (n = 3; mean ± SD). The statistical significance of the differences between the Control and each KD condition (sh*EZH1*, sh*EZH2*, and sh*EZH1/2*) were evaluated by one-way ANOVA followed by Dunnett's multiple comparisons test. ***p < 0.001 *vs.* Control.

Figure S5

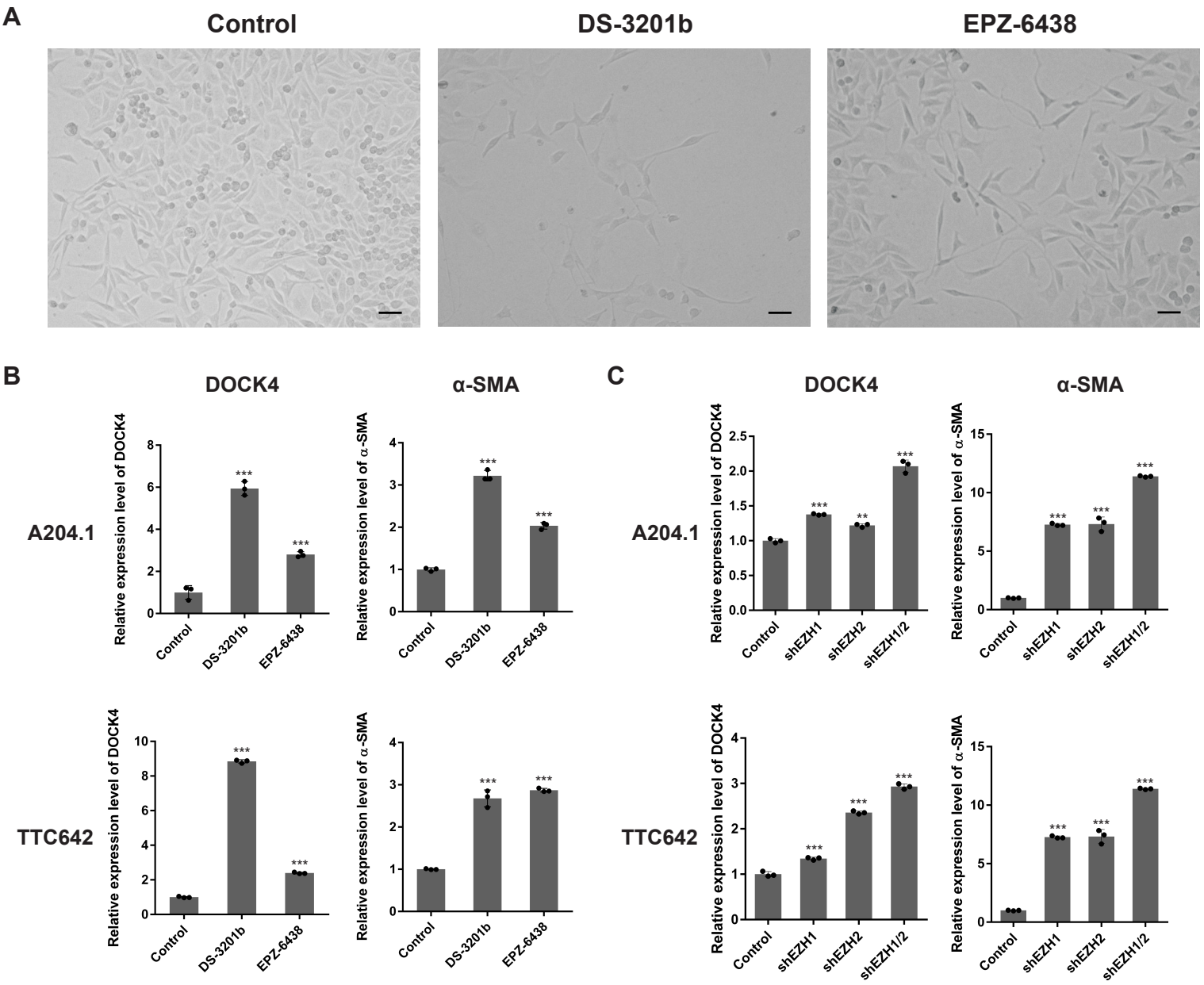

Figure S5. Morphological changes in EZH1/2 dual inhibitor-treated MRT cells.

(A) Representative images showing the morphology of DS-3201b- or EPZ-6438-treated A204.1 cells. Cells were treated with DS-3201b (100 nM) or EPZ-6438 (100 nM) for 7 days, followed by observation under a bright-field microscope. The number of long, thin, spindle-shaped cells increased after treatment with DS-3201b. Scale bars, 50 μm. **(B)** Expression of *DOCK4* and *α-SMA* mRNAs in DS-3201b- or EPZ-6438-treated cells. Cells were treated with DS-3201b (100 nM) or EPZ-6438 (100 nM) for 7 days, followed by qRT-PCR (n = 3, means ± SD). The expression level of the Control is indicated as "1". ***p < 0.001 *vs*. Control. **(C)** Expression of *DOCK4* and *α-SMA* mRNAs in cells in which *EZH1* or *EZH2,* or both, were knocked down (n = 3; mean ± SD). The expression level of the Control is indicated as "1". **p < 0.01, ***p < 0.001 *vs.* Control.

Figure S6

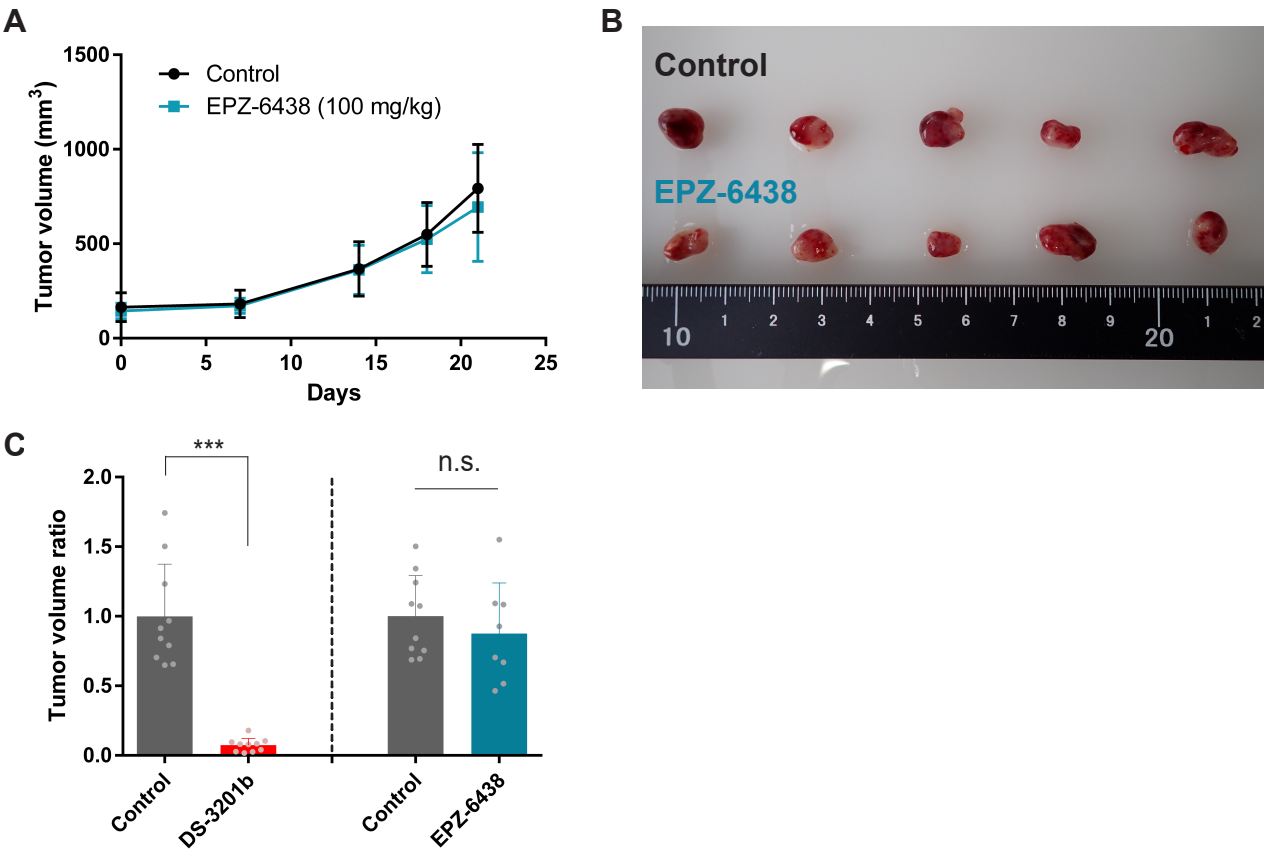

Figure S6. The anti-proliferative effect of an EZH2-selective inhibitor EPZ-6438 in A204.1 xenograft mice.
(A) The tumor volume of A204.1 xenograft mice. A204.1 cells (2×10^6 cells) were suspended in 100 µl of 50% Matrigel prepared in PBS and subcutaneously inoculated into 5-week-old female BALB/c *nu/nu* nude mice. After the mean tumor volume had reached approximately 100 mm^3, the mice were randomized and separated into two groups. The grouping day was set as day 0, and treatment was started at day 1. EPZ-6438 was suspended in 5% DMSO, 40% PEG300, 5% Tween 80, and 50% sterile purified water. The mice were orally administered once daily with 100 mg/kg EPZ-6438 or vehicle control. Differences were statistically evaluated by two-way ANOVA followed by Tukey's multiple comparisons test. The difference between EPZ-6438 and Control was not statistically significant. **(B)** Representative image of tumors from the A204.1 xenograft mice at day 21. **(C)** Tumor volume ratio at day 21. The volume of each Control is indicated as "1". Relative tumor volume of DS-3201b-treated mice is 0.018 and EPZ-6438-treated mice is 0.88. n.s.: not significant, ***$p < 0.001$ *vs.* Control.

Figure S7

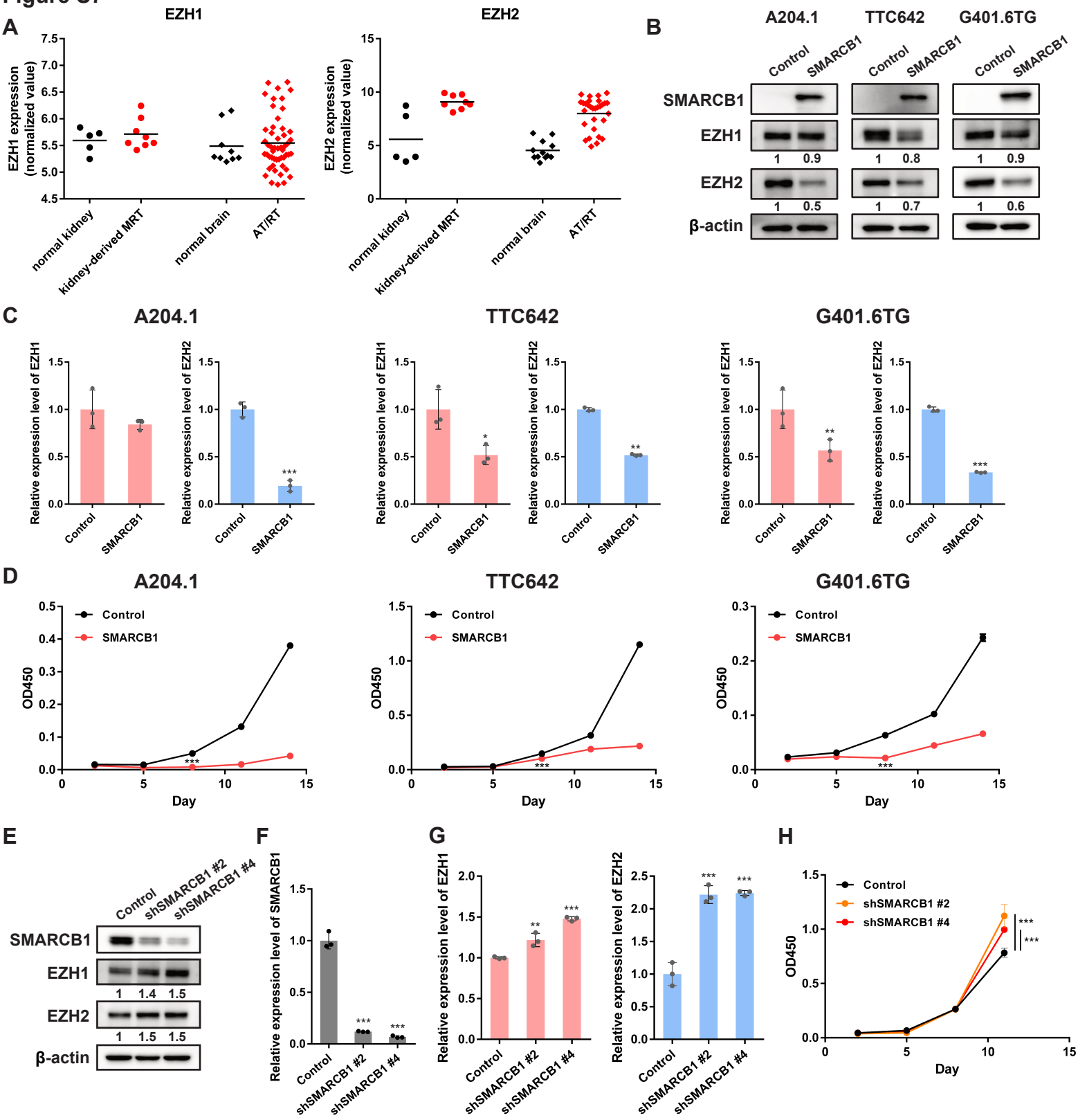

Figure S7. Regulation of EZH1/2 expression by SMARCB1.

(A) Scatter plot of EZH1 and EZH2 expression in primary MRT compared with normal tissues. Gene expression data were obtained from the Gene Expression Omnibus database repository (GEO) and normalized before analysis. Kidney, $p = 0.0425$; Central nervous system, $p = 0.0006$. **(B)** Expression of SMARCB1, EZH1, and EZH2 proteins in SMARCB1-overexpressing cells. Cells were infected with a retroviral SMARCB1 expression vector, and transduced cells were selected by culture with 5 μg/ml of blasticidin for 10 days. Cells were then subjected to western blotting. The numbers below EZH1 and EZH2 indicate each band density relative to Control (taken as "1"). **(C)** Expression of *SMARCB1* mRNA in SMARCB1-overexpressing cells. To confirm overexpression efficacy, the relative expression level of mRNA was evaluated by qRT-PCR ($n = 3$; mean ± SD). The expression level of the Control is indicated as "1". *$p < 0.05$, **$p < 0.01$, ***$p < 0.001$ *vs.* Control. **(D)** Effect of SMARCB1 overexpression on growth of MRT cells. Relative cell growth was measured by a WST-8 assay for the indicated durations ($n = 3$; mean ± SD). Differences were evaluated statistically by two-way ANOVA followed by Tukey's multiple comparisons test. A statistically significant difference between Control cells and SMARCB1-overexpressiong cells was observed on Day 8 (for all cell lines). SMARCB1 *vs.* Control is ***$p < 0.0001$ for all cell lines. **(E–G)** Expression of SMARCB1, EZH1, and EZH2 proteins **(E)** and mRNAs **(F and G)** in *SMARCB1* KD cells. *SMARCB1* wild-type rhabdomyosarcoma RD cells were infected with retroviral sh*SMARCB1* vectors, and transduced cells were selected by culture with 1 μg/ml of puromycin for 3 days. KD efficacy was confirmed by western blotting and qRT-PCR. **(E)** The numbers below EZH1 and EZH2 indicate each band density relative to Control (taken as "1"). **(F and G)** $n = 3$; mean ± SD. The expression level of the Control is indicated as "1". **$p < 0.01$, ***$p < 0.001$ *vs.* Control. **(H)** Effect of *SMACB1* KD on MRT cell growth. Relative cell growth was measured by a WST-8 assay for the indicated durations ($n = 3$; mean ± SD). Differences were evaluated statistically by two-way ANOVA followed by Tukey's multiple comparisons test. A statistically significant difference between the Control and each KD condition (sh*SMARCB1 #2* and sh*SMARCB1 #4*) was observed on Day 11. sh*SMARCB1 #2 vs.* Control is ***$p < 0.0001$, and sh*SMARCB1 #4 vs.* Control is ***$p < 0.0001$.

Figure S8

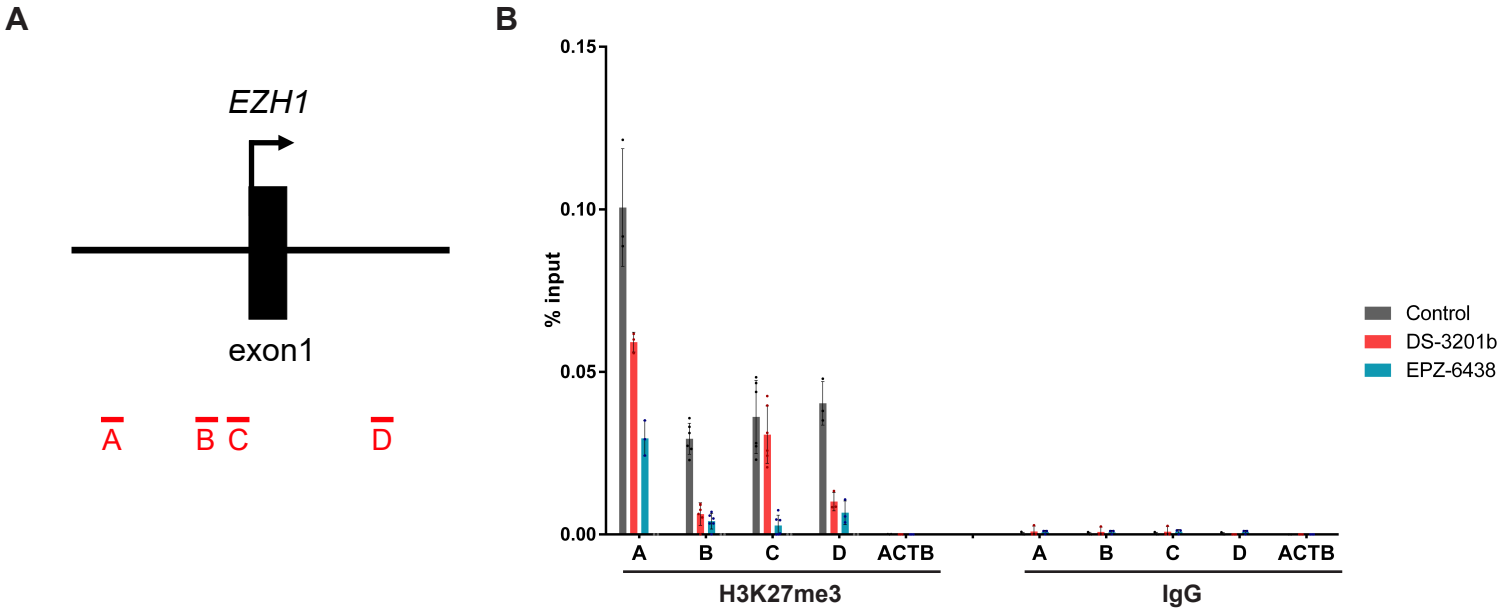

Figure S8. Regulation of EZH1 expression by EZH2.

(A) Schematic of the *EZH1* locus and the locations of the primer pairs used for ChIP-qPCR analysis. **(B)** H3K27me3 enrichment at the *EZH1* locus. A204.1 cells were treated with DS-3201b (100 nM) or EPZ-6438 (100 nM) for 7 days, followed by ChIP-qPCR analysis. Normal rabbit IgG was used as a negative control for the immunoprecipitation. The primer pair specific for ACTB was used as a negative control for the qPCR (n = 6; mean ± SD).

Supplemental Methods

Antibodies

For Western blotting, antibodies against the following proteins were purchased from Cell Signaling Technology (Danvers, MA, USA): EZH1 (#42088), EZH2 (#5246), cleaved Caspase-3 (#9661), PARP-1 (#9542), and SMARCB1 (#91735). Anti-H3K27me3 antibody (07-449) was obtained from Millipore (Billerica, MA, USA). Anti-H3 antibody (ab1791) was purchased from Abcam (Cambridge, MA). The quantity loaded was verified using anti-β-actin antibody (#3700; Cell Signaling Technology).

The following antibodies were used for immunohistochemistry: anti-H3K27me3 (#9733; Cell Signaling Technology), and anti-CDKN2A/p16INK4a (ab108349; abcam).

Vectors

Lentiviral short hairpin RNA (shRNA) vectors (EZH1 #2: TRCN0000002439, EZH1 #5: TRCN0000355735, EZH2 #9: TRCN0000286227, EZH2 #10: TRCN0000293738, SMARCB1 #2: TRCN0000310111, SMARCB1 #4: TRCN0000308015) were obtained from Merck. To generate double knockdown vectors, synthesized oligonucleotides (shEZH1 #2 and shEZH2 #9) were cloned into retroviral vectors pSINsi-DK II (3664; Takara, Otsu, Japan) with promoter cassette. The sequence 5'- CGCTAAATACTGGCAGGCGTT-3' targeting LacZ was used as a negative control. Human *EZH1* cDNA open reading frame (ORF) cloned into a tetracycline-inducible gene expression lentiviral vector (TRE3G-ORF-P2A-eGFP-PGK-Tet3G-bsd) was provided from Transomic Technologies

(Huntsville, AL, USA). Human *SMARCB1* cDNA ORF cloned into lentiviral expression vector (pLOC) was purchased from Horizon Discovery (Cambridge, UK). The virus was produced in 293LT cells transfected using GeneJuice transfection reagent (70967; Merck) with viral constructs along with VSV-G and gag-pol. For lentivirus production, Rev was also co-transfected. To prepare high-titer viral solutions, viral supernatants were collected for two days followed by ultracentrifugation-based concentration at 50,000 × g for 2 h. The titers of viral solutions were confirmed by Lenti-X qRT-PCR Titration Kit (631235; Takara) and Retrovirus Titer Set (6166; Takara), according to the manufacturer's protocols. The lentiviral-mediated GFP expression was analyzed using a JSAN cell sorter (Bay bioscience, Kobe, Japan) and FlowJo software (TreeStar, Ashland, OR, USA). The knockdown and overexpression efficacy were confirmed by immunoblotting and qRT-PCR.

Cell growth assay

For evaluation of the cell proliferation, A204.1, TTC549, and RD cells (1×10^3 cells), G401.6TG, and JMU-RTK-2 cells (5×10^2 cells), and TTC642, and KYM-1 cells (2.5×10^2 cells) were plated in 48 well flat bottom plate at day 1. The basal cell numbers were measured at day 2 by the absorption spectrum of WST-8 formazan dye (OD 450) using a Cell Counting Kit-8 (CK04; Dojindo, Kumamoto, Japan) following the manufacturer's protocol. The relative cell growth was evaluated every 3 days. For assessment of the anti-proliferative effect of inhibitors, the cells were treated with the inhibitors on day 2. The half-maximal inhibitory concentration of the compounds (IC_{50}) was estimated by using

GraphPad Prism 6.0 (GraphPad Software, La Jolla, CA, USA).

Histone protein extraction

Harvested cells were suspended in hypotonic lysis buffer comprising 10 mM Tris-HCl (pH 8.0), 1 mM KCl, 1.5 mM $MgCl_2$, and 1mM DTT containing 1% protease inhibitors (11836170001; Roche, Basel, Switzerland) and 1% phosphatase inhibitors (P5726 and P0044; Sigma-Aldrich, St. Louis, MO, USA). The cells were lysed by 0.1% Triton-X with mechanical shearing and obtained nuclear fractions. The nuclei were incubated with 0.4 N H_2SO_4 overnight at 4°C and the supernatants containing histones were collected, followed by TCA-precipitation.

Reverse-transcription (RT)-PCR

The following probes and primers were used: *ACTB* (Hs03023943_g1); *EZH1* (Hs00940463_m1); *EZH2* (Hs01016789_m1); *CDKN2A* (Hs00923894_m1); *CDKN2C* (Hs00176227_m1); *CDKN1A* (Hs00355782_m1); *SMARCB1*-Fwd, 5'-GGCATCAGAAGACCTACGCCTT-3'; *SMARCB1*-Rev, 5'-CTCCATCTCAGCGTCTGTCAGA-3'; *CD133*-Fwd, 5'-CAGAGTACAACGCCAAACCA-3'; *CD133*-Rev, 5'-AAATCACGATGAGGGTCAGC-3'; *DOCK4*-Fwd, 5'-GCATGTGGATGATTCCCTGCAG-3'; *DOCK4*-Rev, 5'-GGAGGTGATGTAACACGACAGG-3'; *α-SMA*-Fwd, 5'-GTGGCTATTCCTTCGTTACT-3'; *α-SMA*-Rev, 5'-GGCAACTCGTAACTCTTCTC-3'. The level of ACTB mRNA was quantified for internal control.

Gene expression analysis

RNA-sequencing (RNA-seq) analysis was consigned to Kyusyu Pro Search LLP (Fukuoka, Japan). Total RNA samples were extracted using TRIzol (15596026; ThremoFisher) according to the manufacturer's instructions. 500 ng total RNA was ribosomal RNA-depleted using NEBNext rRNA Depletion Kit (E6310; New England Biolabs, Ipswich, MA, USA) and converted to Illumina sequencing library using NEBNext Ultra Directional RNA Library Prep Kit (E7420; New England Biolabs). The library was validated with Bioanalyzer (Agilent Technologies) to determine size distribution and concentration. Paired-end sequencing (2 × 36 bases) was performed with NextSeq 500 sequencer (Illumina, San Diego, CA, USA). Sequence reads were mapped to the human genome (hg19) and quantified for annotated genes by CLC Genomics Workbench (v10.1.1; Qiagen, Venlo, Netherlands). To estimate the expression pattern of transcripts among DS-3201b treatment, EPZ-6438 treatment and control sets, the read counts were normalized by quantile method for total count in individual samples using the CLC Genomics Workbench. Filtering characteristics of FDR adjusted $P < 0.05$ and fold-change > 2 were used to identify the differentially expressed genes. For drawing heatmap and gene enrichment analysis, Log2-converted normalized values were used. Gene enrichment analysis was conducted with Metascape (http://metascape.org.).

Cell cycle analysis

Cell cycle analysis was performed by quantitation of the cellular DNA content with

propidium iodide (PI) staining. DS-3201b- or EPZ-6438-treated cells were harvested at day 8 and 14, and fixed with 70% cold ethanol overnight at 4 °C. The cells were then incubated with RNase A (R4642; Sigma-Aldrich) for 15 min at 37 °C followed by 30 min of staining with PI (421301; Biolegend, San Diego, MA, USA). The stained cells were analyzed by flow cytometry using a JSAN cell sorter. The collected data were analyzed by FlowJo software.

Apoptosis analysis

Apoptotic cells were detected by flow cytometry. DS-3201b- or EPZ-6438-treated cells were harvested at day 14 and stained with Annexin V-APC (640920; Biolegend) and DAPI (D212; Dojindo) in Annexin V binding buffer (422201; Biolegend) at room temperature for 10 min. The stained cells were analyzed using a JSAN cell sorter and FlowJo software.

Chromatin immunoprecipitation (ChIP) assay

Cells (1-5 × 10^7) were cross-linked with 1% formaldehyde at room temperature for 7 min, quenched by adding glycine to 125 mM, and incubated for 10 min on ice. The cells were then incubated with lysis buffer 1 (50 mM HEPES pH 7.5, 100 mM NaCl, 1 mM EDTA, 10% glycerol, 0.5% NP-40, and 0.25% Triton X-100) for 10 min on ice, followed by incubation with lysis buffer 2 (10 mM Tris-HCl pH 8.0, 200 mM NaCl, and 1 mM EDTA) for 10 min on ice. The lysate was resuspended in FA lysis buffer (140 mM NaCl, 1 mM EDTA, 0.1% DOC, 1% TritonX-100, 0.1% SDS, and 50 mM Tris-HCl, pH 7.5) and sonicated using an S220 Focused-ultrasonicator (Covaris, Woburn, MA, USA) to shear chromatin into fragments

with an average length of < 1 kb. After centrifugation, the supernatants were diluted 10-fold with dilution buffer (0.01% SDS, 1% Triton X-100, 2 mM EDTA, 20 mM Tris-HCl pH 8.0, and 150 mM NaCl). The samples were immunoprecipitated with 2 μg of the indicated antibodies overnight at 4°C. Immunocomplexes were pulled down with Dynabeads Protein G (Invitrogen), washed with wash buffer (0.1% SDS, 1% Triton X-100, 2 mM EDTA, 20 mM Tris-HCl pH 8.0, and 150 mM NaCl), and eluted with elution buffer (1% SDS and 0.1 M NaHCO3) for 15 min at 65°C. The cross-links were reversed by incubation with 5 M NaCl overnight at 65°C and continuous incubation with 0.5 M EDTA, 1M Tris-HCl (pH 6.5), and 20 mg/ml proteinase K for 2 h at 55°C. DNA was purified by phenol/chloroform extraction, followed by isopropanol precipitation with Ethachinmate (318-01793; Nippon Gene, Tokyo Japan). The presence of the target gene sequences in both the input DNA and immunoprecipitated DNA was detected by quantitative PCR using gene-specific primers and SYBRGreen (Roche). The following antibodies were used for immunoprecipitation: anti-H3K27me3 (07-449; Millipore), and rabbit IgG (#2729; Cell Signaling Technology). Sequences of the primers used for RT-PCR as follows: *ARF* exon 1β (primer A in Figure 4I)-Fwd, 5'-GTGGGTCCCAGTCTGCAGTTA-3'; *ARF* exon 1β-Rev, 5'-CCTTTGGCACCAGAGGTGAG-3'; 500 bp upstream of *p16-CDKN2A* exon 1α (primer B in Figure 4I)-Fwd, 5'-ACCCCGATTCAATTTGGCAG-3'; 500 bp upstream of *p16-CDKN2A* exon 1α-Rev, 5'- AAAAAGAAATCCGCCCCCG-3'; *p16-CDKN2A* exon 1α (primer C in Figure 4I)-Fwd, 5'-AGAGGGTCTGCAGCGG-3'; *p16-CDKN2A* exon 1α-Rev, 5'-TCGAAGCGCTACCTGATTCC-3'; 350 bp downstream of *p16-CDKN2A* exon 1α

(primer D in Figure 4I)-Fwd, 5'- GCCAAGGAAGAGGAATGAGGAG-3'; 350 bp downstream of *p16-CDKN2A* exon 1α-Rev, 5'-CCTTCAGATCTTCTCAGCATTCG-3'; 2 kb upstream of *EZH1* exon 1 (primer A in Figure S2A)-Fwd, 5'- TCCCTTGCCCCTATCCATTT-3'; 2 kb upstream of *EZH1* exon 1-Rev, 5'- TATCTTGAAGGCAGCGGGAA-3'; 250 bp upstream of *EZH1* exon 1 (primer B in Figure S2A)-Fwd, 5'- TTCAGCGTTTGAAGCCAACC-3'; 250 bp upstream of *EZH1* exon 1-Rev, 5'- AGACCGGTGTCTGGAGAACT-3'; *EZH1* exon 1 (primer C in Figure S2A)-Fwd, 5'- CGCACTACTGTCATTTGCCG-3'; *EZH1* exon 1-Rev, 5'-AGTGGCTCTGCGAAGGTTTC-3'; 2kb downstream of *EZH1* exon 1 (primer D in Figure S2A)-Fwd, 5'-AGCATAAACCTTGACAATGATAGC-3'; 2kb downstream of *EZH1* exon 1-Rev, 5'- GGGAGAGAGAAGTACTTAAAAACGC-3'; *ACTB*-Fwd, 5'-TGTGGACATCTCTTGGGCAC-3'; *ACTB*-Rev, 5'-CAGGAGCGTACAGAACCCAG-.

GEO gene expression data

Gene expression data from kidney derived MRT and normal kidney have been deposited in the Gene Expression Omnibus (GEO) database (GSE11151, and GSE11482). These data sets include: 11 MRTs of the kidney, and 5 normal kidney samples. Gene expression data for 51 AT/RT and 9 pediatric normal brain samples were also downloaded from GEO (GSE35493, and GSE64019). All downloaded data were normalized together using gcRMA (as implemented in Bioconductor).

Immunohistochemistry (IHC)

The tumor tissues from A204.1 xenografted mice were fixed with 4% paraformaldehyde phosphate buffer solution (161-20141; Fujifilm Wako, Osaka, Japan), embedded in paraffin, sectioned, and mounted on microscope glass slides (CRE-01; Matsunami Glass, Osaka, Japan). The slides were deparaffinized in xylene and rehydrated by passage through graded ethanol. For antigen retrieval, the sections were incubated in HistoVT One (#06380-76; Nacalai Tesque) for 20-40 min at 90℃ and cooled down to room temperature. After 3 times wash with diluted water, the sections were blocked with 3% hydrogen peroxide for 10 min, followed by Blocking One Histo (#06349-64; Nacalai Tesque) for 10min. After that, primary antibodies were diluted in Signal Stain Antibody Diluent (#8112; Cell Signaling Technology), added to the sections, and incubated overnight at 4℃. The sections were washed 3 times with TBS-T and incubated with Signal Stain Boost IHC Detection Reagent (HRP, Rabbit, #8114; Cell Signaling Technology) as secondary antibody for 30 min, and then washed 3 times with TBS-T. The signals were visualized with Signal Stain DAB substrate Kit (#8059; Cell Signaling Technology). The slides were counterstained by using hematoxylin (1.09249; Sigma-Aldrich). Histopathological images were acquired by using a BZ-9000 microscope (Keyence, Osaka, Japan). The histopathological sections were reviewed by the American College of Veterinary Pathology (ACVP) or Japanese College of Veterinary Pathology (JCVP)-board-certified veterinary pathologists.